Sustainable Energy, Grids and Networks 32 (2022) 100909

Contents lists available at ScienceDirect

Sustainable Energy, Grids and Networks

journal homepage: www.elsevier.com/locate/segan

Fuzzy logic-based energy management system for grid-connected residential DC microgrids with multi-stack fuel cell systems: A multi-objective approach

F.J. Vivas *, F. Segura, J.M. Andújar

Research Center for Technology, Energy, and Sustainability (CITES), TEP-192 Research Group, University of Huelva, 21007 Huelva, Spain

ARTICLE INFO

Article history:
Received 13 December 2021
Received in revised form 16 July 2022
Accepted 12 August 2022
Available online 19 August 2022

Keywords:
Energy management system
Fuzzy logic controller
Hybrid energy storage system
Multi-stack fuel cell
Multi-objective approach
Renewable microgrid

ABSTRACT

Hybrid energy storage systems (HESS) are considered for use in renewable residential DC microgrids. This architecture is shown as a technically feasible solution to deal with the stochasticity of renewable energy sources, however, the complexity of its design and management increases inexorably. To address this problem, this paper proposes a fuzzy logic-based energy management system (EMS) for use in grid-connected residential DC microgrids with HESS. It is a hydrogen-based HESS, composed of batteries and multi-stack fuel cell system. The proposed EMS is based on a multivariable and multistage fuzzy logic controller, specially designed to cope with a multi-objective problem whose solution increases the microgrid performance in terms of efficiency, operating costs, and lifespan of the HESS. The proposed EMS considers the power balance in the microgrid and its prediction, the performance and degradation of its subsystems, as well as the main electricity grid costs. This article assesses the performance of the developed EMS with respect to three reference EMSs present in the literature: the widely used dual-band hysteresis and two based on multi-objective model predictive control. Simulation results show an increase in the performance of the microgrid from a technical and economic point of view.

1. Introduction

European climate policy focuses its investment on new clean and distributed energy models [1]. With a contribution close to 30%, the residential market is called to play a fundamental role in carbon neutrality and electric vehicle integration [2]. At the residential level, one of the most promising architectures for energy supply is based on the use of renewable-based DC microgrids, with hybrid energy storage systems (HESSs) based on batteries and hydrogen as energy vector [3]. The use of DC buses increases the microgrid performance by allowing direct integration of DC generators and loads, as well as avoiding the problems associated with reactive power and power quality [1].

As for the energy storage system (ESS), batteries usually have a dual function: firstly, they act as a short-term ESS and, secondly, in direct connection topologies, they ensure the stability of the microgrid DC bus voltage. On the other hand, the hydrogen system represents the long-term ESS, and it is usually composed by an electrolyser, a storage tank and a fuel cell (FC), in a simple or modular topology [4]. Compared to the most common mono-stack FC architecture, the use of multi-stack fuel cell (MSFC) systems presents a reliable solution, characterized by redundancy, resiliency, higher efficiency and longer lifetime [5]. Despite their advantages, MSFC systems increase the degrees of freedom and, consequently, the decision possibilities of the energy management system (EMS) of the microgrid, which requires a more complex control [6].

Due to the high number of elements, the high investment cost, as well as the particularities in their operation, hydrogen-based HESS microgrids require a powerful EMS that responds to a complex multi-objective problem whose solution must increase the microgrid performance from a technical and economical point of view [7]. The problems to be solved simultaneously are many, including: ensure power balance, proper HESS management, maintain DC bus voltage operating range, minimize HESS degradation (specifically the hydrogen system) and the cost of connection to the main electricity grid (MEG) [8]. In hydrogen-based HESS systems with MSFC, it is also essential to correctly manage the degradation between the different stacks, usually subjected to different degradation ratios, otherwise their performance and lifespan would be seriously affected [6].

The energy dispatch of HESS-based residential DC microgrids has been widely studied and different EMS solutions have been employed. Among the most used are heuristic techniques (hysteresis and deterministic rule-based methods), model-based techniques (mainly model predictive control (MPC)), and artificial

* Corresponding author.
E-mail address: francisco.vivas@diesia.uhu.es (F.J. Vivas).

https://doi.org/10.1016/j.segan.2022.100909

intelligence-based techniques (basically fuzzy logic (FL)), [9]. As examples of heuristic techniques, in [10–12] a deterministic rule-based strategy is presented in which renewable utilization is maximized for battery charging in the first instance. On the other hand, in [13,14] a dual-band hysteresis-based EMS is used to reduce the degradation associated with the start/stop cycles of the hydrogen system. The main function of the hydrogen system and the MEG is to cope with energy surplus/deficit situations when the battery bank reaches its maximum state of charge (SOC) or charging voltage limit. These techniques are characterized by their simplicity and robustness due to their reduced number of control parameters, however, they do not consider the use of partial loads in the systems, which is essential to increase the microgrid performance [15].

Regarding model-based control techniques, mainly MPC, they have been displacing traditional techniques in all areas, thanks to their ability to solve complex multivariable optimization problems [15]. The performance of these techniques depends on the goodness of the mathematical model, characterized by the strong nonlinearities intrinsic to the components of the microgrid. This requires the use of nonlinear control techniques, which increases the complexity of the control solution, as well as its computational cost [16]. To reduce the complexity of the control problem, the most widespread simplification is the use of linearized models and linear control techniques [17]. Examples of multi-objective techniques based on linear time-invariant (LTI) models are proposed in [18,19], where the power setpoint of the microgrid is calculated to optimize the energy distribution in the short term. To optimize the microgrid response over a longer time horizon, a computationally costly hierarchical EMS is used in [20–22]. An optimal generation scheduling algorithm and an MPC calculate the renewable generation and demand profile forecast, respectively. Based on them, the EMS determines the optimal HESS reference values for the long term. An evolution with respect to previous hierarchical solutions is proposed in [23]. In this work, the use of an event-based MPC is proposed which, depending on the current state of the microgrid, allows the selection among several controllers previously designed to respond to different time horizons. Finally, a MPC controller acts as short-term optimizer and calculates the microgrid power setpoint to track the reference level of the HESS system, while minimizing the degradation and operating costs of the DC microgrid. Despite the advantages of these techniques, none of the proposed works guarantee real DC bus voltage control (only SOC is controlled), include loss reduction among their design objectives, or propose the use and management of MSFC systems. Likewise, the simplification of the microgrid model can negatively affect the EMS response in real systems, providing a suboptimal solution to the control problem, even going as far as the insolubility of the actual control problem [24].

There is probably no better technique for dealing with complex models and uncertainties than FL. This allows the control problem can be faced without an explicit model of the plant. Instead, the model is replaced by easily interpretable linguistic rules [25]. On the other hand, FL allows the incorporation of expert knowledge about the plant under control into the rules of the fuzzy inference system, which usually facilitates the solution of the problem [26]. This was the rationale behind the decision to use a fuzzy logic controller (FLC) to implement the EMS in this work.

In this sense, FL has proven to be an excellent technique for the design of complex EMS for use in renewable microgrids with different architectures and in different applications. Thus, [27] proposes the use of a decentralized FLC for the energy management of a grid-connected renewable microgrid used as an electric vehicle charging station, with an architecture based on a DC bus and batteries as ESS. Specifically, the FLC ensures power balancing, prioritizing the use of the microgrid resources over the use of the MEG, while guaranteeing the operating limits of the SOC and the DC bus voltage. In [28], a low-complex FL-based EMS is used on a grid-connected residential microgrid with renewable generation and battery-based ESS. The objective of the designed FLC is to minimize the fluctuations in the energy exchange between the microgrid and the MEG, considering as inputs the SOC of the battery bank and the forecast error in the generation and demand profiles. A more complex microgrid architecture and control problem is studied in [29], where a domestic hot water (DHW) thermal system is included in the microgrid. In this case, the DHW water temperature is added to the usual objectives.

For similar architectures to the microgrid under study, different FL-based solutions have been found in the scientific literature depending on the application. In terms of economic optimization, the solutions found are diverse. In [30], an optimized FLC based on genetic and evolutionary algorithms is designed to reduce the operating cost of the MEG and operating hours of HESS, considering the time-varying MEG prices and the intermittency of renewable generation. The control algorithm is based on the prediction of the microgrid cost and the stored energy in the HESS (hydrogen level (HL)). Finally, in [31] a FLC determines the power setpoint of the MEG and HESS with the objective of keeping the level of the stored energy of the HESS close to its design level while minimizing the operation and maintenance (O&M) costs of the microgrid. For this purpose, a cost function that includes the HESS operating and depreciation costs is used.

The problem of microgrid DC bus voltage management with ESS support is studied in [32], where a robust type-3 FLC is used in the control of the different power converters of the renewable generators and HESS, with the aim of regulating the DC bus voltage in the presence of high variability renewable generation. Similarly, in [33], a FL-based EMS determines, based on the microgrid power balance and the stored energy of the HESS, the power setpoint of the hydrogen system to solve the DC voltage regulation problem of a supercapacitor-supported DC bus. Finally, in [34], a FLC is designed to regulate the voltage and frequency in a hybrid DC/AC microgrid architecture. In this case, the FLC is successfully applied in the control of different DC/DC and DC/AC power converters.

A technique to increase the lifespan of the HESS is presented in [35], in which a FLC considers the degradation associated with the hydrogen system operating cycles and determines, based on the power balance prediction, the most favourable start-up and shutdown conditions. A similar solution is used in [36], which presents an EMS based on two-time horizons, in which a FLC acts as a short-term EMS, and implements a hysteresis cycle to reduce the degradation associated with the hydrogen system cycling. A different approach is taken in [37], where a complex FL-based multilevel controller is successfully applied in a renewable microgrid with battery-based HESS, superconducting magnetic ESS and hydrogen as energy vector. A FLC acts as master level control and provides the HESS power setpoint. This setpoint ensures power balance, while making conservative use of the HESS by reducing the number of unnecessary operating cycles of the hydrogen system, and operating the battery bank with reduced depth of discharge (DOD). The slave (local) controllers are implemented using a first-order sliding mode control based on a nonlinear barrier function, which imposes the power setpoint of the HESS on its respective power converter.

A technique to maximize hydrogen generation is studied in [38]. Specifically, a passive FLC is used for the energy management of an isolated renewable microgrid, which aims to maximize renewable hydrogen generation through optimal energy sharing between the battery and the hydrogen system. In this

case, the controller inputs are defined by the generation and demand profiles, the HL, and the battery SOC.

Finally, taking into account the performance of the microgrid, there are works that prioritize control actions to improve the efficiency of the hydrogen cycle. Thus, in [39], it is presented an EMS whose objective is to operate a FC stack at its maximum efficiency point. On the other hand, in [40], a more complex microgrid architecture is evaluated, in which an osmosis plant is available to supply pure water to the electrolyser. The implemented control law makes use of partial loads for the equipment. On the other hand, in [41], the use of a hybrid FL-based EMS and optimization techniques (artificial bee colony) is proposed for a battery-supported DC bus microgrid, in which the calculation of the HESS power setpoint optimizes its efficiency, and in the ultimately the cost of connection to MEG. A FL-based EMS for grid-connected microgrid is presented in [42]. The principal novelties of this work with respect to [42], among others, are: a MSFC system is used; the multi-objective function integrates terms associated with HESS performance; the microgrid loads increase; the control architecture uses two parallel controllers that compute the entire parameter vector; an event-based controller determines the output vector of the FLC depending on the sign of the power balance; a local controller supervises the MSFC system management; and, in addition, a performance comparison against other EMS present in the literature is carried out.

In summary, the novelty of this work can be condensed into the following aspects:

1. Comprehensive management of a complex residential microgrid architecture that includes renewable generation, demand profiles associated with household appliances (HA), heating, ventilation and air conditioning (HVAC), electric vehicle (EV) charging point, medium voltage DC bus supported by the direct connection of a battery bank, and a HESS based on batteries and hydrogen as an energy vector, consisting of an electrolyser, a hydrogen tank and an MSFC system. That is, the complete hydrogen cycle (production, storage and utilization) is carried out within the microgrid.
2. An active FL-based EMS with a novel parallel structure has been developed to control the microgrid under study in both the short and long term. The FLC design approach responds to a multi-objective problem whose individual objectives are to ensure the safe, economical, and efficient operation of the microgrid; while at the same time achieving a very high degree of independence from the MEG by taking advantage of the microgrid architecture and its own resources, as well as controlling the DC bus voltage and increasing the lifespan of the HESS. To achieve this, the FLC inputs are defined by the energy stored in the HESS (HL and SOC), the current DC bus voltage, the power balance and its prediction, the accumulated degradation in the equipment, the efficiency in the operation of the HESS and the cost of connections to the MEG.
3. A new FL-based EMS for energy management of an MSFC system. The developed FLC allows to increase the lifespan of the MSFC system by making a more conservative use, reducing the number of operating cycles, and ensuring a uniform long-term degradation of the different stacks that make up the MSFC system.
4. Long-term simulations have been performed for different real scenarios in order to validate the performance of the developed FLC architecture. The results have been compared with respect to three reference EMSs present in the literature and widely used.

Finally, to highlight the novelty of the research, Table 1 summarizes the main characteristics of the authors' proposal in comparison with the analysed literature.

This document is organized as follows: Section 2 describes the architecture and model of the microgrid. Section 3 explains the developed EMS, its structure, the fuzzy sets and the fuzzy rule bases. Section 4 presents the performance of the developed EMS as well as its comparison with the reference ones present in the literature. The results obtained are discussed in Section 5. Finally, the main conclusions are presented in Section 6.

2. Microgrid description

2.1. Microgrid architecture, sizing and design criteria

The objective of this study is the development of a multi-objective FL-based EMS for a grid-connected residential DC microgrid with HESS. This is based on the microgrid located at the University of Huelva (Spain), Fig. 1. More details as well as the development of the mathematical model of this microgrid can be found at [8,19].

The microgrid is based on a 360 VDC battery supported DC bus, see Fig. 1. As the renewable energy source, a 10 kWp photovoltaic (PV) field is available and connected to the DC bus through a DC/DC converter [43] that implements maximum power point tracker algorithm, specifically a modified perturbation and observation (P&OM) algorithm [44]. The required PV power has been calculated by simulations based on the daily PV generation profiles of the site, as well as the expected demand, obtained from the Institute for Energy Diversification and Saving of Spain (typical consumption of a single-family house plus additional power for the production of renewable hydrogen and an electric car recharging point). Please, see section results for more details regarding renewable generation and consumptions in the microgrid. The integration of all consumptions in the microgrid has been carried out by means of appropriate power converters, Fig. 1.

The proposed ESS is based on the concept of system hybridization, i.e., using systems with different but complementary characteristics and dynamics to best meet the hourly power and energy requirements of the microgrid.

As a short-term response ESS, a 36 kWh lead–acid battery bank is used. The energy storage capacity of the battery bank has been calculated to ensure sufficient capacity to absorb generation and demand power peaks without abrupt change in its SOC, which would result in large voltage variations on the DC bus. Note, in Fig. 1, that the lead–acid battery bank is directly connected to the DC bus, so it is the guarantor of its voltage. This allows all generators in the microgrid to work against the DC bus using MPPT algorithms in their power converters, instead of algorithms that regulate the output voltage.

The hydrogen system is designed to perform the function of a long-term ESS. It is made up of a 1 N m^3/h alkaline electrolyser, a 1 N m^3-30 bar hydrogen storage tank and a 6 kW MSFC system, consisting of a proton-exchange membrane (PEM) fuel cell with two stacks connected in parallel, each of which can have different degradation. The rated power of the electrolyser responds to the maximum installed PV power. This sizing criterion allows taking advantage of the maximum renewable resource, since there are hours of maximum photovoltaic generation with minimum domestic consumption, which is the best time to produce renewable hydrogen.

The rated power of each MSFC stack has been selected based on the availability of commercial solutions and, of course, under the criterion that the MSFC can comfortably satisfy the maximum instantaneous power demand so that it can be met using only the hydrogen resource. The MSFC stacks chosen are air-cooled, due to its reduced balance of plant, lower cost and easy management [6].

Table 1
Comparison of the findings of the proposed paper with the previously analysed literature.

EMS	Ref.	Objective	Decision Parameters	Decision making	HESS configuration
Rule-based strategy	[10–12]	– Ensuring power balance	– Power balance – SOC, HL – DC bus voltage	– Short term	– Battery – Electrolyser – Single-stack FC
Dual-band hysteresis	[13,14]	– Ensuring power balance – Conservative use of HESS	– Power balance – SOC, HL	– Short term	– Battery – Electrolyser – Single-stack FC
MPC	[18–23]	– Ensuring power balance – Conservative use of HESS – O&M Cost reduction	– Power balance – Energy forecast – SOC, HL – MEG cost – HESS degradation	– Short term – Long-term	– Battery – Electrolyser – Single-stack FC
Fuzzy Logic Controller	[27]	– Ensuring power balance – Conservative use of ESS – DC bus voltage control	– Power balance – SOC – DC bus voltage	– Short term	– Only battery
	[28]	– Ensuring power balance – Conservative use of ESS – Minimize fluctuations in the MEG profile	– Power balance – SOC – Forecast error	– Short term	– Only battery
	[29]	– Ensuring power balance – Conservative use of ESS – Minimize fluctuations in the MEG profile	– Power balance – SOC – Forecast error – Water temperature	– Short term	– Only battery
	[30,31]	– O&M Cost reduction	– Power balance – Energy forecast – SOC, HL – MEG cost	– Short term – Long-term	– Battery – Electrolyser – Single-stack FC
	[32–34]	– DC/AC bus voltage control	– Power balance – SOC, HL – DC bus voltage	– Short term	– Battery – Electrolyser – Single-stack FC
	[35,36]	– Conservative use of HESS	– Power balance – Energy forecast – SOC, HL – HESS degradation	– Short term – Long-term	– Battery – Electrolyser – Single-stack FC
	[37]	– Ensuring power balance – Conservative use of ESS	– Power balance – SOC, HL	– Short term	– Battery – Superconducting magnetic ESS – Electrolyser – Single-stack FC
	[38]	– Ensuring power balance – Hydrogen generation maximization	– Power balance – SOC, HL	– Short term	– Battery – Electrolyser – Single-stack FC
	[39–41]	– Reduction of energy losses	– Power balance – Energy forecast – SOC, HL – MEG cost – HESS efficiency	– Short term – Long-term	– Battery – Electrolyser – Single-stack FC
	[42]	– Ensuring power balance – Conservative use of HESS – O&M Cost reduction – DC bus voltage control	– Power balance – Energy forecast – SOC, HL – MEG cost – HESS degradation – DC bus voltage	– Short term – Long-term	– Battery – Electrolyser – Single-stack FC
	Author's proposal	– Ensuring power balance – Conservative use of HESS – O&M Cost reduction – DC bus voltage control – Reduction of energy losses	– Power balance – Energy forecast – SOC, HL – MEG cost – HESS degradation – DC bus voltage – HESS efficiency	– Short term – Long-term	– Battery – Electrolyser – MSFC system

On the other hand, the capacity of the hydrogen storage tank has been sized considering the availability of commercial solutions that guarantee a stored energy equivalent to an average autonomy of 8 h of continuous operation of the MSFC system, enough to guarantee the demand profile during the hours when there is no renewable generation. In this regard, it should be noted that except when the electric vehicle is being recharged, it is sufficient to keep a single stack running to meet the demand. Please see the results section for more details regarding this.

Finally, the microgrid has a bidirectional connection point with the MEG, in order to be able to exchange energy with it (buy/sell).

The main characteristics of the components that make up the microgrid are shown in Table 2. The power converters have been designed and developed by the authors to have full control of the devices (commercial ones, if suitable, are closed and do not allow modifications of the control system and firmware. The authors have a great deal of experience in this field, for example, see [45].

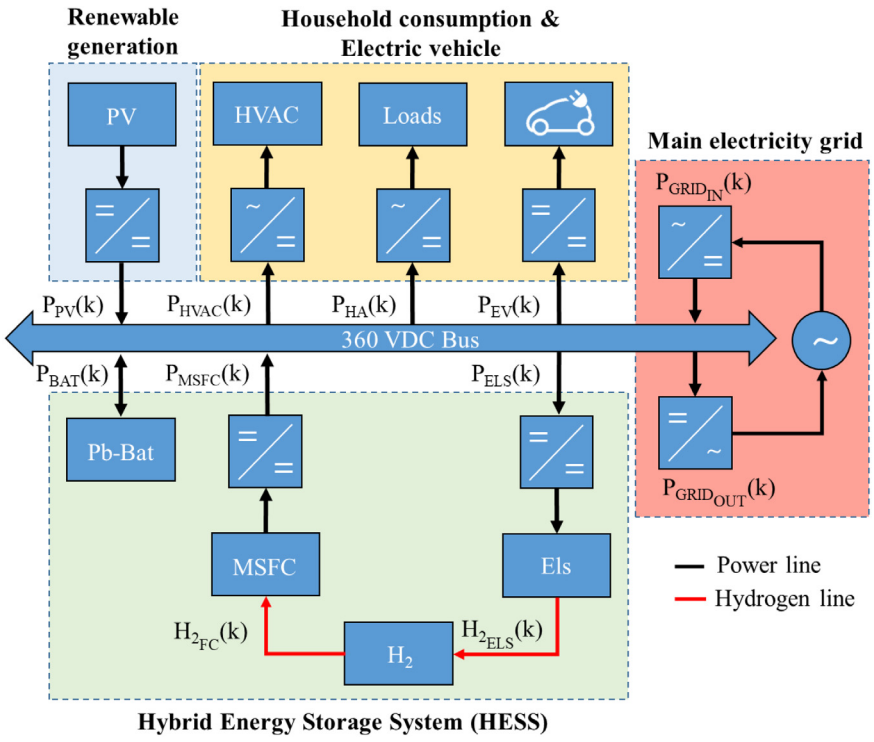

Fig. 1. Architecture of the residential microgrid under study.

Table 2
Technical characteristics of the microgrid subsystems.

Component	Manufacturer	Nominal parameters
Solar PV mono-Si	ISOFOTON® ISF-250	10 kW $_p$
Electric Vehicle	Nissan® Leaf	30 kWh
Lead–acid battery bank	U-POWER® UP100-12	30 x 12 V, 100 Ah (36 kWh)
Alkaline Electrolyser	ARIEMA®	1 N m^3/h, 10 kWe
PEM fuel cell stacks	Ballard® FCgen-1020ACS	2 x 3 kW $_p$
Hydrogen storage tank	Lapesa® LSP1000H	1.044 N m^3, 30 bar

2.2. Modelling

This subsection describes the microgrid model. This model has already been presented in previous works [8,19] so only its basic characteristics will be reported here. Nevertheless, it is very important to note that the proposed FL-based EMS does not require a microgrid model, which is probably the most important advantage compared to other EMSs. However, as is obvious, in order to carry out the simulations and comparisons with the rest of the EMS analysed, it is necessary to have the microgrid model. This explains the wording of this subsection.

(A) Power Balance on the DC Bus

The power balance is defined as the difference between the renewable generated and demanded, and must be guaranteed at all times by the HESS and/or the MEG [19]. According to Fig. 1, the power balance on the DC bus must comply with (1). The sign criterion adopted is that any power injected into the DC bus is considered positive, while any power demanded is considered negative.

$$P_{BAL}(k) = P_{PV}(k) - \left(\underbrace{P_{HVAC}(k) + P_{HA}(k) + P_{EV}(k)}_{P_{LOAD}(k)} \right) = \underbrace{P_{BAT}(k) + P_{H_2}(k)}_{P_{HESS}(k)} + P_{Grid}(k) \quad (1)$$

According to Fig. 1, $P_{H_2}(k)$, $P_{BAT}(k)$ and $P_{Grid}(k)$ can be expressed as (2).

$$P_{H_2}(k) = \begin{cases} P_{ELS}(k), & P_{H_2}(k) < 0 \\ P_{MSFC}(k), & P_{H_2}(k) \geq 0 \end{cases}$$
$$P_{Grid}(k) = \begin{cases} P_{GRID_{OUT}}(k), & P_{Grid}(k) < 0 \\ P_{GRID_{IN}}(k), & P_{Grid}(k) \geq 0 \end{cases} \quad (2)$$

$P_{BAT}(k) < 0$ in charge and $P_{BAT}(k) \geq 0$ in discharge

(B) Battery Bank

To increase the techno-economic performance of the microgrid, the available power of the battery bank will be calculated based on its voltage, state of charge (SOC), degradation and losses.

– Battery Voltage

Based on the battery technology, Copetti's proposal [46] is used to model its voltage. The model parameters were obtained through an experimental identification process and can be found in [8].

– State of Charge

The battery SOC is defined from the charge balance and sign criteria ($P_{BAT}(k) < 0$ char., $P_{BAT}(k) > 0$ disc.) according to the Coulomb counting method [47], as shown in (3).

$$SOC(k+1) = SOC(k) - \frac{\eta_{BAT}(k) \cdot I_{BAT}(k) \cdot T_s}{C_N(k)} \quad (3)$$

Where $\eta_{BAT}(k)$ is the overall battery efficiency at sampling k (%), $I_{bat}(k)$ is the battery current at sampling k (A), T_s is the sampling time and $C_N(k)$ is the rated battery capacity at sampling k (Ah).

– Battery Degradation

The battery degradation (D_{BAT}) is obtained from the experimental curve of capacity loss regarding the number of operating cycles. For this purpose, a linear relationship is defined based on a degradation parameter (α), which quantifies the relationship between the maximum capacity loss, which determines the end of lifespan, and the expected amount of energy for a design deep of discharge (DOD). [8]. See (4).

$$D_{BAT}(k+1) = D_{BAT}(k) + \frac{\alpha \cdot \eta_{BAT}(k) \cdot |I_{BAT}(k)| \cdot T_s}{C_N(k)} \tag{4}$$

C) Hydrogen System

According to the microgrid architecture (Fig. 1), one of the EMS roles is to ensure proper use of the hydrogen system. To this end, the electrolyser and MSFC power setpoint must be calculated based on the hydrogen generation/consumption ratio, their degradations, and the operating losses.

– Hydrogen Level

The hydrogen level (HL) is calculated from the hydrogen balance, defined by the hydrogen generated and consumed by the electrolyser ($H2_{ELS}$) and the MSFC ($H2_{FC}$, as it is independent for each stack) respectively, as expressed in (5).

$$HL(k+1) = HL(k) + (H2_{ELS}(k) - H2_{FC}(k)) \tag{5}$$

– Hydrogen Generation/Consumption

The hydrogen generation or consumption by the electrolyser or MSFC ($H2_x(k)$), respectively, is proportional to the operating current according to Faraday's Law [48,49], as shown in (6).

$$H2_x(k) = \frac{\dot{n_{H2}}(k) \cdot M_{H2}}{\rho_{H2}} = \frac{P_x(k) \cdot N_{cell(x)} \cdot M_{H2}}{z \cdot F \cdot \rho_{H2} \cdot V_x(k)} \cdot T_s;\ x = ELS\ or\ FC \tag{6}$$

Where $\dot{n_{H2}}(k)$ is the hydrogen production/consumption ratio (N m^3/h) at sampling time k, M_{H2} is the molecular hydrogen molar mass (2.02 g/mol), ρ_{H2} is the molecular hydrogen gas density (0.0899 kg/N m^3), $P_x(k)$ is the operating power associated to electrolyser (ELS) or fuel cell (FC) at sampling time k (W), $N_{cell(x)}$ is the number of cells of the electrolyser (ELS) or fuel cell (FC), z is the number of electrons involved in the reduction–oxidation reaction ($z = 2$), F is the Faraday constant (26.81 Ah/eq) and $V_x(k)$ the operating voltage of the electrolyser (ELS) or fuel cell (FC).

The operating voltages of the electrolyser and fuel cell can be obtained from their polarization curves as a function of the operating power.

– Hydrogen System Degradation

The electrolyser degradation (D_{ELS}) is quantified as a function of the number of operating equivalent hours at rated conditions, (7). On the other hand, the degradation of each MSFC stack (D_{FC}) is determined from the number of ON/OFF cycles and the equivalent operating time at rated conditions [8], as described in (8).

$$D_{ELS}(k+1) = \sum \frac{P_{ELS}(k) \cdot T_s}{P_{ELS_N}} \tag{7}$$

$$D_{FC}(k+1) = \Delta V_{CYC} \cdot CYC_{FC}(k) + \sum \Delta V_{TIME} \frac{P_{FC}(k) \cdot T_s}{P_{FC_N}} \tag{8}$$

Where P_{ELS_N} and P_{FC_N} are, respectively, the electrolyser and each MSFC stack, ΔV_{CYC} is the voltage drop of each stack considering the operating cycles (V/cycle/cell), $CYC_{FC}(k)$ is the number of operating cycles of each stack at sampling k and ΔV_{TIME} the voltage drop of each stack considering the operating hours (V/h/cell).

Table 3
Model parameters of the microgrid subsystems.

Param.	Value	Param.	Value
α	7.58 $\cdot 10^{-4}$ Ah	$D_{FC_{Max}}$	100 mV/cell
η_{BAT}	85%	$\Delta V_{CYC_{FC1}}$	48 μV/cycle/cell
η_{GRID}	95%	$\Delta V_{CYC_{FC2}}$	60 μV/cycle/cell
$D_{BAT_{Max}}$	20 Ah	$\Delta V_{TIME_{FC1}}$	9 μV/h/cell
$D_{ELS_{Max}}$	10000 h	$\Delta V_{TIME_{FC2}}$	12 μV/h/cell

– Hydrogen System Efficiency

The efficiency of the electrolyser and of each stack in the MSFC (η_{ELS} and η_{FC} respectively) are defined by the ratio of the hydrogen chemical power generated/consumed and the electrical power consumed/generated [8]. See (9) and (10).

$$\eta_{ELS}(k) = \frac{P_{H_2ELS}(k)}{P_{ELS}(k)} = \frac{H_{2ELS}(k) \cdot LHV}{P_{ELS}(k)} \tag{9}$$

$$\eta_{FC}(k) = \frac{P_{FC}(k)}{P_{H_2FC}(k)} = \frac{P_{FC}(k)}{H_{2FC}(k) \cdot LHV} \tag{10}$$

Where LHV is the hydrogen lower heating value (2993 Wh/N m^3).

D) Microgrid Cost

Assuming as negligible the O&M cost in comparison with the economic amount of the purchase/sale of energy from MEG, the microgrid operating cost (C_{MICRO}) is given by (11).

$$C_{MICRO}(k+1) = T_s \cdot (P_{GRID_{IN}}(k) \cdot C_{EP}(k) + P_{GRID_{OUT}}(k) \cdot C_{ES}(k)) \tag{11}$$

Where $C_{EP}(k)$ is the cost of purchasing energy from the MEG at sampling k (€/Wh) and $C_{ES}(k)$ the cost of selling energy to the MEG at sampling k (€/Wh). In what follows, the word cost of the MEG will always be used, whether energy is being sold or bought.

E) Microgrid Losses

The significant microgrid losses ($Loss$) are determined by the losses of the HESS and the MEG [8], due to the electronic devices connecting both grids, calculated from their operating power and efficiency, as shown in (12).

$$Loss(k+1) = \sum P_x(k) \cdot \left(\frac{1-\eta_x(k)}{\eta_x(k)}\right);\ x = BAT, ELS, FC, GRID \tag{12}$$

Finally, the main parameters of the microgrid systems are collected in Table 3.

3. EMS design based on fuzzy logic

This section presents a FL-based EMS design to solve the multi-objective problem of the correct operation of the microgrid in Fig. 1. This requires ensuring the power balance while seeking to reduce HESS degradation, energy losses, and the MEG cost. The actions to be carried out are detailed below.

Direct connection of the battery bank to the DC bus ensures voltage stability but makes it a more vulnerable system. To prolong its lifetime, it is mandatory to set limitations for the charging and discharging process, mainly, to establish a voltage-controlled charging protocol and to limit the DOD.

As shown in Fig. 1, the hydrogen ESS consists of an electrolyser and a MSFC system. Unlike the first one, fuel cells have a reduced lifetime, which is highly dependent on the operating conditions. Similarly, the use of MSFC systems requires local control actions to avoid disparate degradation between stacks, which would reduce the benefits of this architecture [6]. In addition, the hydrogen cycle is characterized by low efficiency. To address both problems, it is necessary to consider their operating power, number of cycles and operating time.

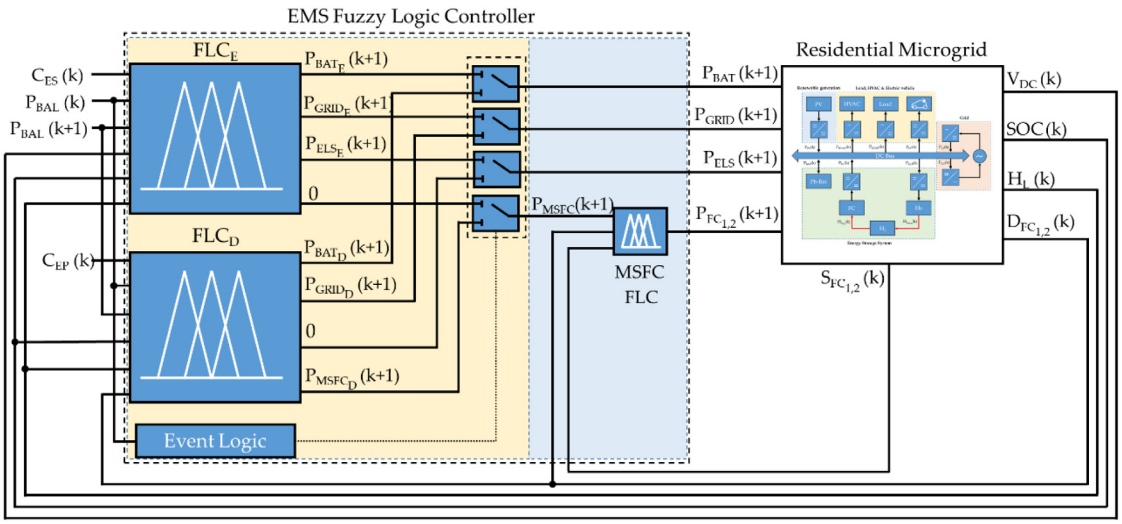

Fig. 2. EMS control structure. (For interpretation of the references to colour in this figure legend, the reader is referred to the web version of this article.)

Finally, in pursuit of an economic objective, it is necessary to make advantageous use of the MEG. For this purpose, the microgrid power setpoint must be calculated based on the stored energy (SOC and HL), the power balance, its prediction, and the cost of connection to the MEG.

In the following sections, the FLC will be explained step by step.

3.1. Fuzzy logic controller structure

The proposed FL-based EMS is shown in Fig. 2. Since the operation of the HESS and the interaction with the MEG are directly dependent on the power balance, the EMS design has been defined based on two FLC, one for energy excess situations (FLC_E) and another for energy deficit situations (FLC_D). This architecture allows, on the one hand, to adapt the response of the microgrid to the energy situation at any given moment, since a situation of excess or deficit of energy will condition the operation of the HESS and the connection to the MEG, while at the same time allowing to solve the complex problem associated with energy management by dividing it into two simpler subproblems.

In this architecture, both controllers will operate in parallel, and an event-based controller will be used to determine the FLC output variables set depending on the sign of the power balance (centralized EMS, Fig. 2, salmon-coloured zone).

Finally, to increase the lifetime of the MSFC system, a local FLC has been specially designed. This FLC calculates the operating power of each stack according to their accumulated degradation (MSFC FLC Fig. 2, blue-coloured zone).

As previously explained, it is crucial to ensure that the battery SOC and voltage are within their operating limits. Regarding the system topology, Fig. 1, perfect synchronism is required by the rest of the equipment to guarantee the surplus/deficit energy is properly managed. According to the above, $V_{BAT}(V_{DC})$ and SOC must be defined as input variables of the EMS controller, while P_{BAT} will be a controller output. Depending on the sign of the power balance, P_{BAT} will be defined by P_{BAT_E} (FLC_E controller output variable) or P_{BAT_D} (FLC_D controller output variable), if the system is in an energy surplus or deficit situation, requiring the charging or discharging of the battery bank respectively.

Regarding the HESS architecture, Fig. 1, the hydrogen system operates as a long-term ESS. Thus, during an energy excess situation, the controller allows the energy surplus to be used to produce hydrogen by means of the electrolyser. In the case of an energy deficit situation, the stored hydrogen can be used to produce electric power by means of the MSFC system. For this, the HL must be within the operating limits. To increase the HESS lifetime, the MSFC degradation must be considered to realize the proper energy distribution between the HESS and the MEG. According to the above, HL and $D_{FC1,2}$ must be defined as input variables of the EMS controller, while P_{ELS} and P_{MSFC} will be outputs of the controller. Depending on the energy situation of the microgrid, corrective actions to ensure power balance should be different. Thus, with respect to the hydrogen system, for a situation of energy surplus (P_{BAL}> 0 according to (1)), the FLC_E controller will calculate the power setpoint of the element that will allow the excess energy to be absorbed, therefore it will calculate the electrolyser power setpoint (P_{ELS_E}), while the MFSC system will remain off, since it acts as a source. On the contrary, during an energy deficit situation (P_{BAL} < 0 according to (1)), the FLC_D controller will calculate the power setpoint of the element that allows compensating the energy deficit, and therefore it will calculate the power setpoint of the MSFC system (P_{MSFC_D}), while the electrolyser, which acts as a load, will remain off.

In addition, the MEG connection can be used to balance the operating costs of the microgrid, as well as to ensure power and energy balance in unfavourable situations. Therefore, it is the power and energy situation of the microgrid (SOC, HL, the power balance, and its forecast), and the MEG cost which will determine its power setpoint. Then P_{BAL}, P_{BAL}(k+1), C_{EP} and C_{ES}, must be defined as input variables of the EMS controller. On the other hand, P_{GRID} will be a controller output. Depending on the power balance sign, P_{GRID} will be defined by P_{GRID_E}(FLC_E controller output variable) or P_{GRID_D}(FLC_D controller output variable), if the microgrid is in a situation of energy surplus or deficit, respectively, requiring the sale or purchase of energy from the MEG, also respectively.

Finally, the MSFC FLC acts as a local EMS (Fig. 3), which sets the power setpoint of each stack based on the EMS controller's MSFC power setpoint, their cumulative degradation, and their current operating state ($S_{FC1,2}$(k)).

The fuzzy rule base of the FLC is designed to reduce the number of operating cycles in the event of power balance disturbances, and to increase the lifespan of the MSFC system by matching the operating power to the current degradation of each stack. According to the above, P_{MSFC}, $D_{FC1,2}$ and $S_{FC1,2}$ must be defined as input variables of the MSFC controller, while $P_{FC1,2}$ will be the controller outputs.

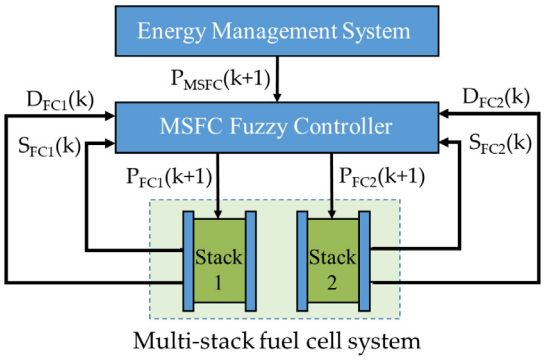

Fig. 3. Block diagram and FLC architecture for the MSFC system.

Table 4
Universe of discourse of fuzzy variables.

Variable	Lower limit	Upper limit	Variable	Lower limit	Upper limit
$C_{ES}(k)$	0.03 €/kWh	0.08 €/kWh	$P_{BAL}(k+1)$	−10 kW	10 kW
$C_{EP}(k)$	0.03 €/kWh	0.12 €/kWh	$P_{MSFC}(k)$	0 kW	6 kW
$DFC_{1,2}(k)$	0 mV/cell	100 mV/cell	$SFC_{1,2}(k)$	0 kW	3 kW
$HL(k)$	3 N m^3	20 N m^3	$SOC(k)$	50%	90%
$P_{BAL}(k)$	−10 Kw	10 kW	$V_{BAT}(k)$	330 V	420 V

3.2. Fuzzy sets

From the knowledge of the microgrid, the design criteria explained and the behaviour shown by the FLC in different simulations, fuzzy sets have been defined, using triangular and trapezoidal membership functions of unit scale (Fig. 4). The number of membership functions is given by adequately covering the universe of discourse of the variables, so that smooth control actions are generated. Of course, it is not an optimal number, but the result of different tests.

The universe of discourse of each fuzzy variable has been delimited based on the safe operation limits to guarantee the correct operation of the microgrid, and the manufacturers' specifications. These limits are listed in Table 4.

Regarding Table 4, the universe of discourse of the power balance and its forecast will be given by situations in which renewable generation is maximum, and demand is zero, and vice versa.

The SOC limits have been determined heuristically, based on simulations with the goal of reaching a commitment between extending battery lifespan by using a reduced DOD, and setting a conservative upper limit to avoid overcharging, at the same time that it pursues to make a conservative use of the hydrogen system. On the other hand, battery voltage operating limits are set by the safe voltage range defined by the manufacturer, as well as by the operating range of the DC bus of the microgrid, in order to guarantee the adequate integration of all the equipment.

As for the hydrogen system, the storage capacity of the hydrogen tank is set to avoid full discharge, possible outside air pollution, and overpressure. Regarding the power of the MSFC system, its limit is determined by the nominal power of each stack (2 *x* 3 kW). As for the maximum degradation of the stack, it is determined by the manufacturer at 100 mV/cell. Reaching this value determines a very important loss of stack performance and, consequently, the condition of the end of its lifespan.

Finally, the discourse universe of the cost of purchasing energy from the MEG is variable and is defined by the prices established in the Spanish electricity market in each auction.

3.3. Fuzzy rule base

Based on the proposed controller structure and the membership functions presented in Fig. 4, three fuzzy rule bases have been defined (one for each controller). Regarding the number of rules of each one, the objective is to cover the dynamics of all the situations of the microgrid (it is really about making a heuristic model), so that the EMS always knows what to do. Again, as in the case of membership functions, it is not an optimal number but also the result of different tests.

FLC_E, FLC_D and MSFC FLC are defined by 41, 42 and 27 rules respectively, listed in Tables 5–7. For their understanding, the behaviour of the microgrid in excess/deficit energy situations will be described below.

3.3.1. Energy excess situation

In this situation, the EMS aims to ensure the power balance and maximize the renewable resource by storing energy or selling it to the MEG. Then, in FLC_E, Fig. 2, the energy distribution between the HESS and the MEG will be determined by the power balance, its prediction, the DC bus voltage (V_{Bat}), the stored energy (SOC and HL) and the energy selling price. The premises for its calculation are ordered according to their priority: maintaining the DC bus voltage within the safe operating range, guaranteeing the energy reserve in the HESS when its value is low or when a deficit power balance is expected, as well as obtaining an economic return when conditions are more favourable.

For the DC bus voltage control, a constant voltage charging protocol is established, posing a tracking problem according to the battery charge acceptance curve. Ultimately, the MEG will ensure the power balance when the HESS is no longer able to absorb energy.

Based on the described operation and the fuzzy rule base defined for the FLC_E controller, Fig. 5 shows the controller output surface for both electrolyser and MEG power.

3.3.2. Energy deficit situation

In the case of energy deficit (FLC_D), Fig. 2, the objective of the EMS is to guarantee the power balance, prioritizing the use of stored energy over the use of the MEG, while making conservative use of the HESS system.

The energy distribution between the HESS and the MEG will be determined by the power balance, its prediction, the accumulated degradation of the stacks, the stored energy and the energy purchasing price. The premises for its calculation are ordered according to their priority: prioritizing the use of batteries as a short-term ESS, guaranteeing the HESS operating limits, conservative use of the MSFC system, and ensuring maximum independence from the MEG to reduce system costs. Despite this premise, depending on the energy situation and the electricity market, a new energy distribution may be considered. Thus, the energy input from the MEG will be assessed if the purchase price and the energy stored in the microgrid are low and an energy deficit situation is expected.

From the power setpoint of the MSFC system, the MSFC controller performs the corresponding energy share between stacks, prioritizing the one with the lowest cumulative degradation. To do this, the local EMS increases the stack power setpoint with the least degradation and maintains its operation over time if the demand profile is reduced or fluctuating, avoiding harmful operating cycles. Ultimately, the MEG will ensure the power balance when the HESS is no longer able to supply energy.

Figs. 6 and 7 shows the controllers output surface for MSFC and grid power and the output surface for the FC1,2 power respectively.

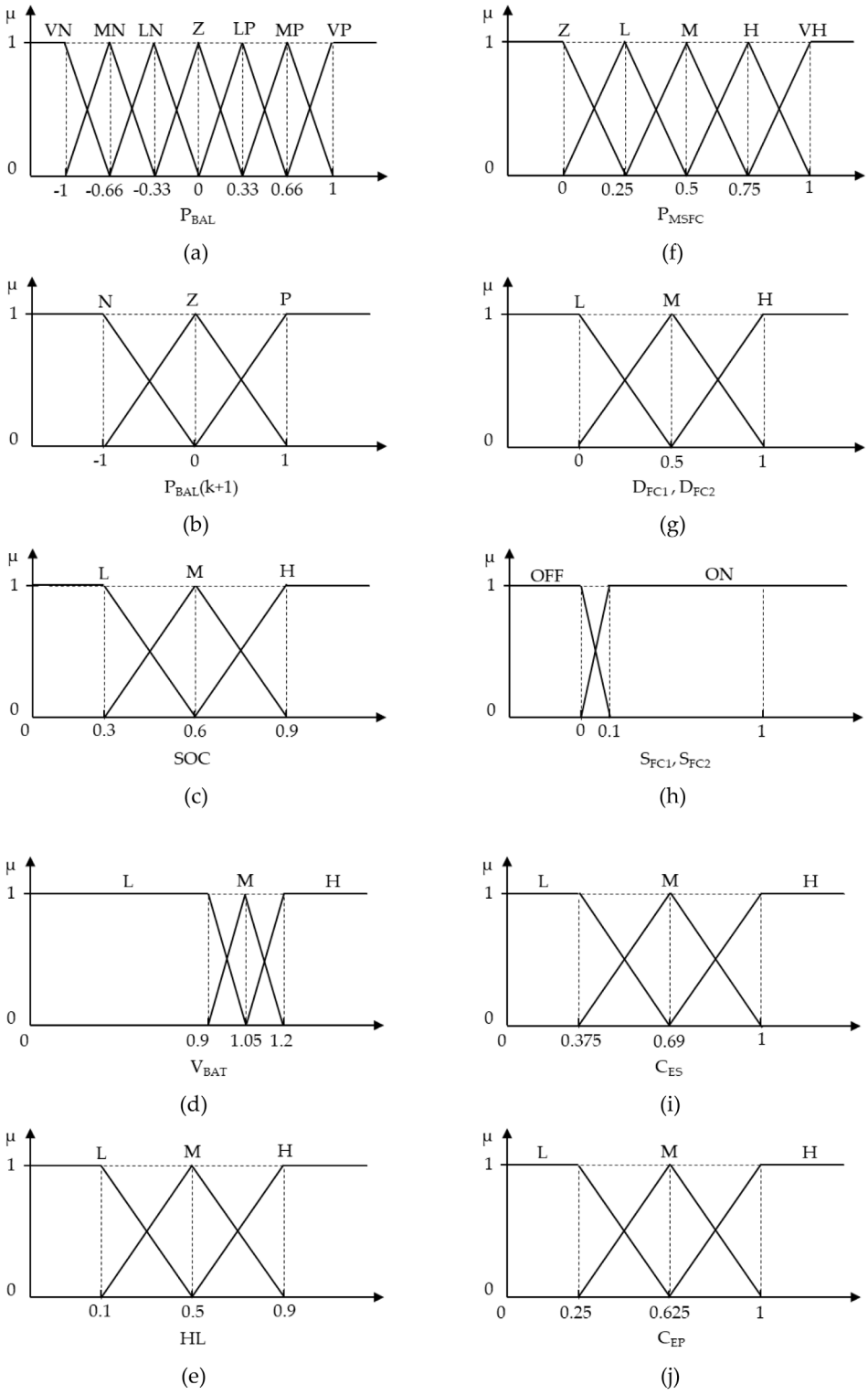

Fig. 4. Membership functions of (a) P_{BAL}; (b) $P_{BAL}(k+1)$; (c) SOC; (d) V_{BAT}; (e) HL; (f) P_{MSFC}; (g) $D_{FC1,2}(k)$; (h) $S_{FC1,2}(k)$; (i) C_{EP}; (j) C_{ES}.

4. Results

The residential microgrid location under study is Huelva, in the southwest corner of Spain, at 37° latitude in the northern hemisphere. The climate of the area is typical subtropical. Specifically, according to the Köppen–Geiger climate classification, it is included in the Csa climate zone: Temperate and rainy winters, dry and hot summers and variable springs and autumns, both in terms of temperature and rainfall. The data of the typical consumption of a single-family house plus the additional power for an electric car recharging point have been provided by the Institute for the Diversification and Saving of Energy of Spain [50].

To validate the developed EMS, several simulations have been performed in the MATLAB® environment for the microgrid architecture modelled in section 2.2 (in more detail in [8]) and

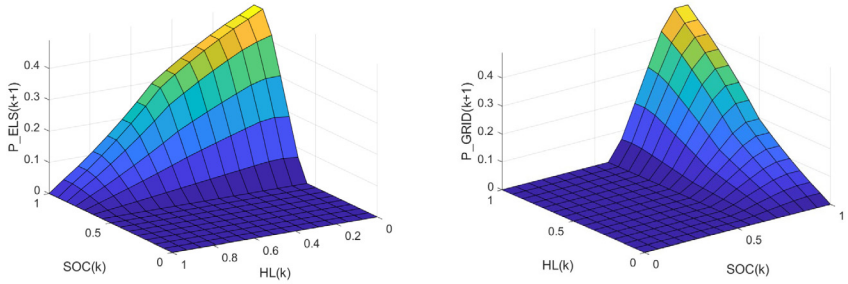

Fig. 5. (a) FLC output surface for P_{ELS} regarding HL and SOC; (b) FLC output surface for P_{GRID} regarding HL and SOC.

Table 5
Fuzzy rule base of the FLC_E controller.

Inputs variables						Output variable		Inputs variables						Output variable	
SOC	HL	P_{BAL}	P_{BAL} (k+1)	C_{ES}	V_{BAT}	P_{ELS}	P_{GRID}	SOC	HL	P_{BAL}	P_{BAL} (k+1)	C_{ES}	V_{BAT}	P_{ELS}	P_{GRID}
–	–	Z	–	–	–	0	0	M	M	MP	N	L	H	0.66	0
L	–	–	–	–	∼H	0	0	M	M	VP	N	L	H	1	0
M	–	–	–	–	V	0	0	M	M	LP	N	∼L	H	0	0.33
M	–	LP	–	–	M	0	0	M	M	MP	N	∼L	H	0	0.5
M	H	MP	–	–	M	0	0.33	M	M	VP	N	∼L	H	0	1
M	H	HP	–	–	M	0	0.66	H	H	LP	–	–	–	0	0.33
M	H	LP	–	–	H	0	0.33	H	H	MP	–	–	–	0	0.66
M	H	MP	–	–	H	0	0.66	H	H	VP	–	–	–	0	1
M	H	VP	–	–	H	0	1	H	L	LP	–	–	–	0.33	0
M	L	MP	–	–	M	0.33	0	H	L	MP	–	–	–	0.66	0
M	L	VP	–	–	M	0.66	0	H	L	VP	–	–	–	1	0
M	L	LP	–	–	H	0.33	0	H	M	LP	N	–	–	0.33	0
M	L	MP	–	–	H	0.66	0	H	M	MP	N	–	–	0.66	0
M	L	VP	–	–	H	0.7	0	H	M	VP	N	–	–	1	0
M	M	MP	N	–	M	0.33	0	H	∼M	LP	∼N	L	–	0.33	0
M	M	VP	N	–	M	0.66	0	H	∼M	MP	∼N	L	–	0.66	0
M	M	M	∼N	L	M	0.33	0	H	∼M	VP	∼N	L	–	1	0
M	M	VP	∼N	L	M	0.66	0	H	∼M	LP	∼N	∼L	–	0	0.33
M	M	MP	∼N	∼L	M	0.66	0	H	∼M	MP	∼N	∼L	–	0	0.66
M	M	VP	∼N	∼L	M	0	0.66	H	∼M	VP	∼N	∼L	–	0	1
M	M	LP	N	L	H	0.33	0								

Table 6
Fuzzy rule base of the FLC_D controller.

Inputs variables						Output variable		Inputs variables						Output variable	
SOC	HL	P_{BAL}	P_{BAL} (k+1)	C_{EP}	D_{MSFC}	P_{MSFC}	P_{GRID}	SOC	HL	P_{BAL}	P_{BAL} (k+1)	C_{EP}	D_{MSFC}	P_{MSFC}	P_{GRID}
H	–	–	–	–	–	0	0	M	–	MN	P	H	H	0	0.25
∼L	–	0	–	–	–	0	0	M	∼L	MN	∼P	–	∼H	0.5	0
L	–	Z	P	–	–	0	0	M	L	MN	∼P	∼H	–	0	0.75
L	∼L	Z	∼P	–	∼H	0.5	0	M	L	MN	∼P	H	–	0	0.5
L	L	Z	∼P	∼H	–	0	0.5	M	–	MN	∼P	∼H	H	0	0.75
L	L	Z	∼P	H	–	0	0.25	M	–	MN	∼P	H	H	0	0.5
L	–	Z	∼P	∼H	H	0	0.5	L	∼L	MN	–	–	∼H	0.75	0
L	–	Z	∼P	H	H	0	0.25	L	L	MN	–	∼H	–	0	0.75
M	–	LN	P	–	–	0	0	L	L	MN	–	H	–	0	0.5
M	∼L	LN	∼P	–	∼H	0.25	0	L	–	MN	–	∼H	–	0	0.75
M	L	LN	∼P	–	–	0	0.25	L	–	MN	–	H	H	0	0.5
M	–	LN	∼P	–	H	0	0.25	M	∼L	VN	–	–	∼H	0.75	0
L	∼L	LN	–	–	∼H	0.5	0	M	L	VN	P	–	–	0	0.75
L	L	LN	–	∼H	–	0	0.5	M	–	VN	P	–	H	0	0.75
L	L	LN	–	H	–	0	0.5	M	L	VN	∼P	∼H	–	0	1
L	–	LN	–	∼H	H	0	0.5	M	L	VN	∼P	H	–	0	0.75
L	–	LN	–	H	H	0	0.25	M	–	VN	∼P	∼H	H	0	1
M	∼L	MN	P	–	∼H	0.25	0	M	–	VN	∼P	H	H	0	0.75
M	L	MN	P	∼H	–	0	0.5	L	∼L	VN	–	–	∼H	1	0
M	L	MN	P	H	–	0	0.25	L	L	VN	–	–	–	0	1
M	–	MN	P	∼H	H	0	0.5	L	–	VN	–	–	H	0	1

shown in Fig. 1. A sampling time of 2 min has been used in the simulations.

Fig. 8 shows the first day of simulation, January 1, a day with continuous cloud passage, as reflected by the generated renewable power (PPV). This Figure only represent the renewable energy generation in the microgrid and the residential consumption profile, not the dynamics of microgrid operation. The consumption profile corresponds to the degree of use of the dwelling. Normally the residents are at home first thing in the morning, from noon to early afternoon and from mid-afternoon onwards.

Table 7
Fuzzy rule base of the MSFC controller.

Inputs variables					Output variable		Inputs variables					Output variable	
P_{MSFC}	D_{FC1}	D_{FC2}	S_{FC1}	S_{FC2}	P_{FC1}	P_{FC2}	P_{MSFC}	D_{FC1}	D_{FC2}	S_{FC1}	S_{FC2}	P_{FC1}	P_{FC2}
Z	–	–	–	–	0	0	L	H	H	ON	ON	0.5	0
VH	–	–	–	–	1	1	M	L	L	–	–	0.5	0.5
L	L	L	–	OFF	0.5	0	M	L	∼L	–	–	1	0
L	L	L	OFF	ON	0	0.5	M	∼L	L	–	–	0	1
L	L	L	ON	ON	0.5	0	M	M	M	–	–	0.5	0.5
L	L	∼L	–	–	0.5	0	M	M	H	–	–	1	0
L	∼L	L	–	–	0	0.5	M	H	M	–	–	0	1
L	M	M	–	OFF	0.5	0	M	H	H	–	–	0.5	0.5
L	M	M	OFF	ON	0	0.5	H	L	–	–	–	1	0.5
L	M	M	ON	ON	0.5	0	H	∼L	L	–	–	0.5	1
L	M	H	–	–	0.5	0	H	M	∼L	–	–	1	0.5
L	H	M	–	–	0	0.5	H	H	M	–	–	0.5	1
L	H	H	–	OFF	0.5	0	H	H	H	–	–	1	0.5
L	H	H	OFF	ON	0	0.5							

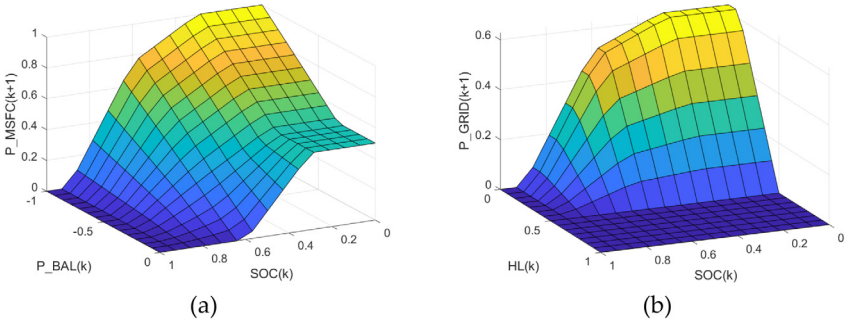

Fig. 6. (a) FLC output surface for P_{MSFC} regarding P_{BAL} and SOC; (b) FLC output surface for P_{GRID} power regarding P_{BAL} and HL.

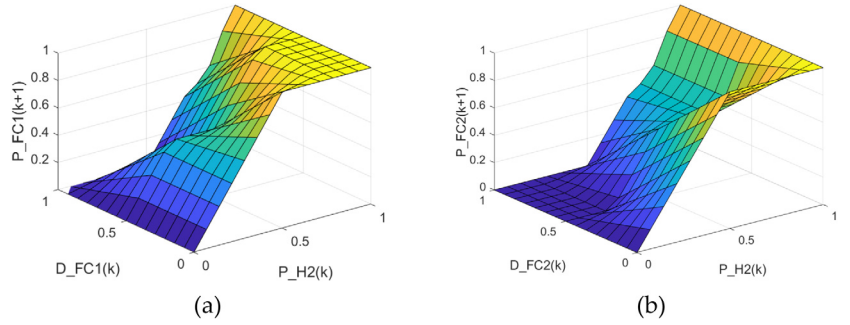

Fig. 7. (a) FLC output surface for FC1 regarding P_{MSFC} and DFC_1; (b) FLC output surface for FC2 regarding P_{MSFC} and DFC_2..

This explains the peaks and valleys of consumption. Specifically, the continuous peaks and valleys of HVAC (heating mainly at this time of the year) correspond to reaching the setpoint temperature. Regarding electric car recharging, it takes advantage of the time of least consumption in the dwelling and when, in addition, electricity is cheaper. Fig. 9 shows the energy purchase price from MEG, which corresponds to the price established by the Spanish electricity market for a typical tariff with hourly discrimination. However, the selling price of energy is fixed at −0.06 €/kWh. Of course purchase and sale prices are constantly changing and the EMS must be informed of this.

To show a realistic simulation scenario, daily on-site renewable generation profiles (updated every two minutes) have been considered together with monthly consumption profiles, logically adapted to the time of the year. In order to clearly appreciate the evolution of the deterioration of the stacks, a long-term simulation of almost two years has been considered.

The simulation aims to evaluate the behaviour of the FL-based EMS in the microgrid under study (Fig. 1), both in the short-term (minutes), considering generation and demand profiles (Fig. 8 shows one day as an example), and in the long-term (months), considering the impact that the evolution of the HESS degradation will have on the microgrid's setpoints. Specifically, it is desired to evaluate the performance of the EMS according to the proposed multi-objective problem, in such a way that the power balance is always guaranteed, correct battery bank charge/discharge management is applied and therefore the DC bus voltage is controlled, there is a technical–economic commitment to the use of MEG, and an increase in the lifespan of the HESS is observed through conservative use of the batteries, electrolyser and MSFC system.

Fig. 10 shows the dynamics of the microgrid managed by the developed EMS, both in the short and long term.

Fig. 10(a) shows the photovoltaic generation (PPV) and the residential consumption profile (first day of simulation, that is,

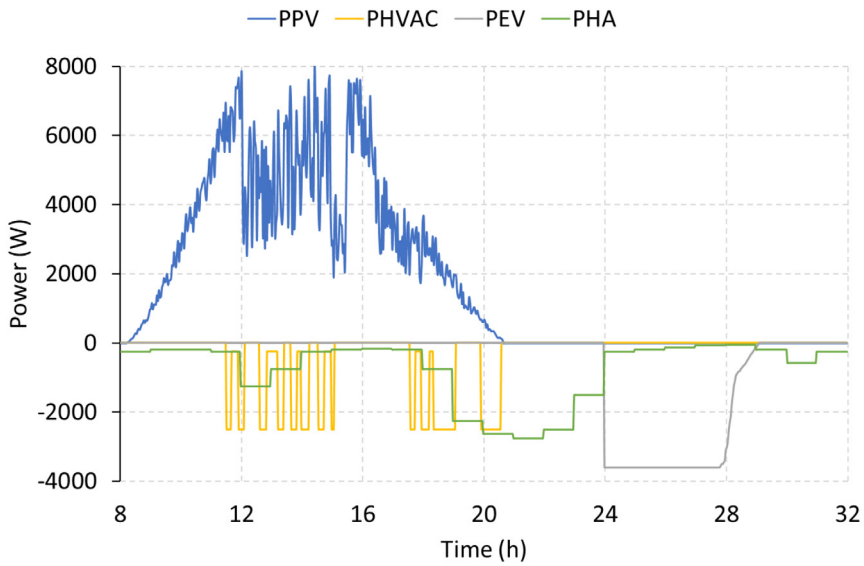

Fig. 8. Renewable energy generation in the microgrid and residential consumption profile: renewable power (PPV), HVAC, EV and home appliances demand (PHVAC, PEV and PHA respectively).

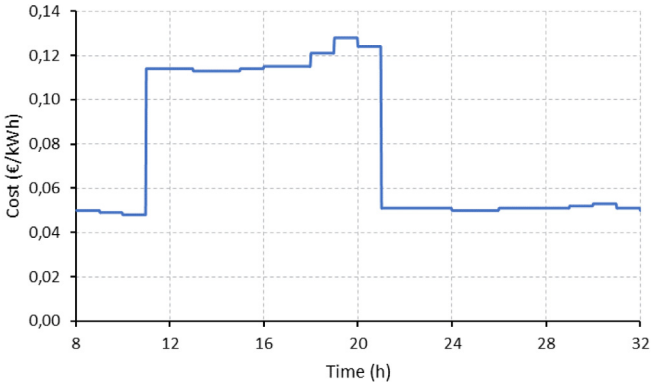

Fig. 9. Daily profile of the cost of energy purchases from MEG.

analogous to Fig. 8) managed by the developed EMS. PLOAD represents the sum of all residential loads (PHA+PHVAC+PEV), with a negative sign according to Eq. (1). Together with the aforementioned variables, those that affect the HESS are represented, namely, the battery bank power (PBAT), positive or negative, if the battery is in discharge or charge mode, respectively; and the hydrogen system power (PH2), defined as the sum of the electrolyser power (negative) and the MSFC system power (positive), according to Eq. (2). Finally, the power profile of the MEG (PMEG) is shown, positive or negative, in case of purchase or sale of energy to the MEG, respectively.

Fig. 10(b) shows the dynamic of the microgrid 670 days after Fig. 10(a). The explanation as to why that particular number of days will be given later in this section. Of course, PV generation and residential consumption are different in both figures. The second one is about a fairly sunny autumn day.

Fig. 11 shows, for the developed EMS, the energy stored in the HESS at the beginning and at the end of the time considered.

To validate the performance of the developed EMS, it has been compared with three reference EMSs under the same initial conditions and with the same generation and demand profiles. In the first instance, with respect to a widely used dual-band hysteresis EMS [51] (hyst-based EMS), and then with respect to two multi-objective MPC model-based EMS (MPC-based EMS). Both EMSs propose a multi-objective optimization based on cost reduction and conservative use of hydrogen system. The difference between them lies in the priority objective. One of them aims to minimize operating costs [52] (MPC-based EMS1), while the other seeks to increase the systems lifespan [53] (MPC-based EMS2). The main parameters that define the EMSs presented in [51–53] are listed in Table 8.

As none of the compared EMS discriminates the power of each stack of the MSFC system, in the simulations an equal power distribution between its two stacks was assumed. The simulation time will be determined by the case in which the lifespan limit of any of the stacks of the MSFC system is reached first. In this case 671 days (16104 h), which explains the time scale in Fig. 10. Note in Fig. 12 that it is stack 2 (DFC2) that is the first to become unusable when the EMS governing the microgrid is Hyst-based EMS.

To validate the battery bank charge management strategy, Fig. 13 shows the DC bus voltage profile of the microgrid for all the EMSs compared. Finally, Table 9 summarizes the main technical and economic parameters obtained after completion of the simulation.

5. Discussion

Figs. 5, 6 and 7 provide important information regarding the problem addressed in this paper. On the one hand, they show that microgrid control is a nonlinear problem, with the very important connotations of complexity that this entails. On the other hand, they also show that the performance of the controllers is smooth, which gives an idea of a good choice of the membership functions, their distribution in the universe of discourse of each variable, as well as the construction of the fuzzy rule bases to contain (model) the complete dynamics of the microgrid.

Figs. 8 and 9 are merely descriptive/informative and are not the result of the research carried out.

Figs. 10 (a) and (b) show the behaviour of the microgrid as a function of the health of the MSFC system, i.e., in 10 (a) at the beginning of the stacks' lives, and 10 (b) at the end.

According to the generation and consumption profile, Fig. 10, the microgrid is in energy surplus in the time slots: 9 h $\leq t \leq$ 17 h in Fig. 10(a), and 16081 h $\leq t \leq$ 16090 h in Fig. 10(b).

The developed EMS uses the energy surplus in the first instance to charge the battery bank, with the aim of guaranteeing a

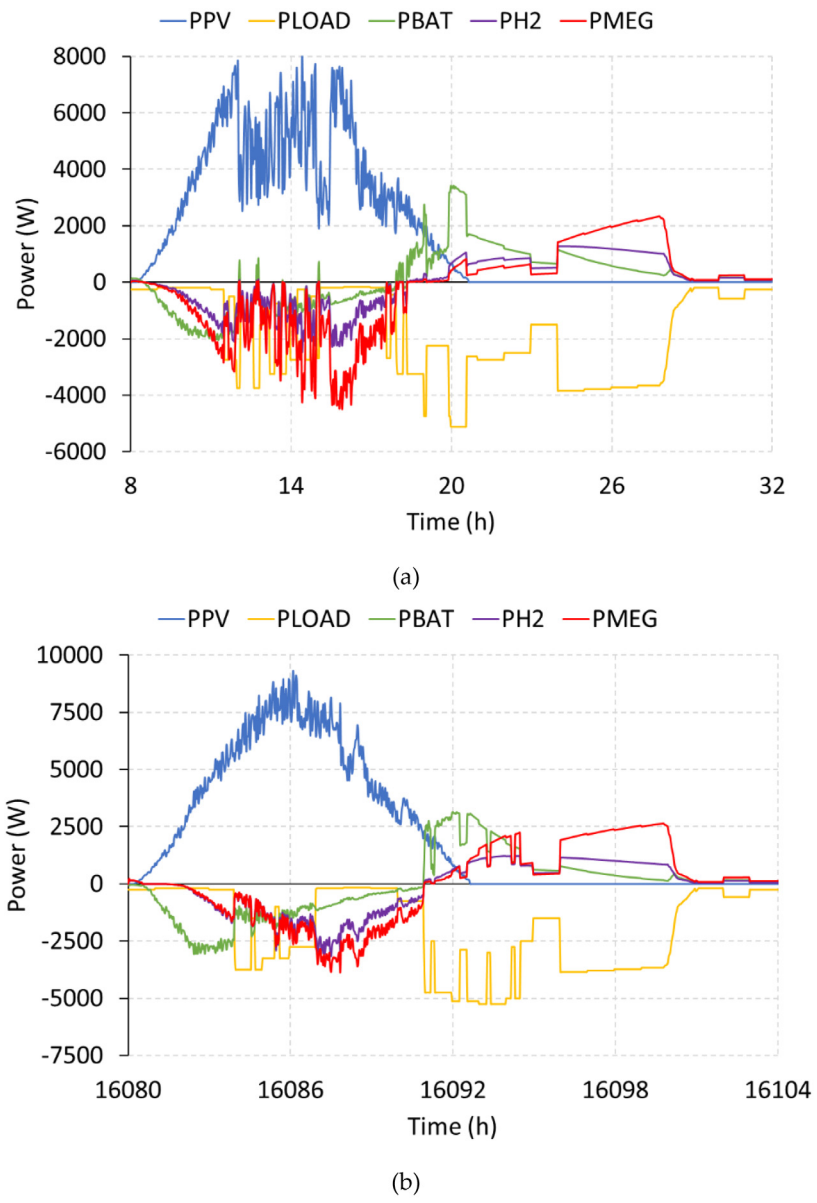

Fig. 10. Dynamics of the microgrid managed by the developed EMS: renewable power (PPV), power demanded (PLOAD = PHA + PHVAC + PEV), PBAT, PH2 and PGRID for (a) 8 h $\leq t \leq$ 32 h; and (b) 16080 h $\leq t \leq$ 16104 h.

Table 8
Hyst-based and MPC-based EMS parameters.

Hyst-based EMS		MPC-based EMS		
Parameter	Value	Parameter	Parameter	Constraints
Minimum SOC threshold	50%	N_P	5	-10 kW $\leq P_{BAT}/\Delta P_{BAT} \leq$ 10 kW
Maximum SOC threshold	90%	N_U	2	-10 kW $\leq P_{H2} \leq$ 6 kW
Hysteresis bandwidth	10%	SOC_{Ref}	60%	-2 kW $\leq \Delta P_{H2} \leq$ 2 kW
Electrolyser power setpoint	10 kW	HL_{Ref}	13.5 N m^3	-10 kW $\leq P_{GRID}/\Delta P_{GRID} \leq$ 10 kW
MSFC power setpoint	6 kW			

SOC and bank battery voltage (DC bus voltage) close to the maximum design values. For this purpose, the EMS determines the energy required for the charging process, establishing a voltage-controlled charging protocol. Thus, the battery bank is charged efficiently and safely, keeping the SOC and DC bus voltage within the desired limits, see Fig. 13(a) and (b) for 9 h $\leq t \leq$ 17 h and 16081 h $\leq t \leq$ 16090 h, respectively, as well as Fig. 13.

The remaining surplus energy is shared between the hydrogen system and the MEG, according to the microgrid energy status and the cost of selling energy to the MEG: 9 h $\leq t \leq$ 17 h in Fig. 10(a), and 16081 h $\leq t \leq$ 16090 h in Fig. 10(b). Thus, if the hydrogen level is medium (10 N m^3 $\leq$ HL (k) $\leq$ 20 N m^3), the developed EMS assesses the cost of selling energy to the grid and, in a favourable case, it performs an equal power distribution

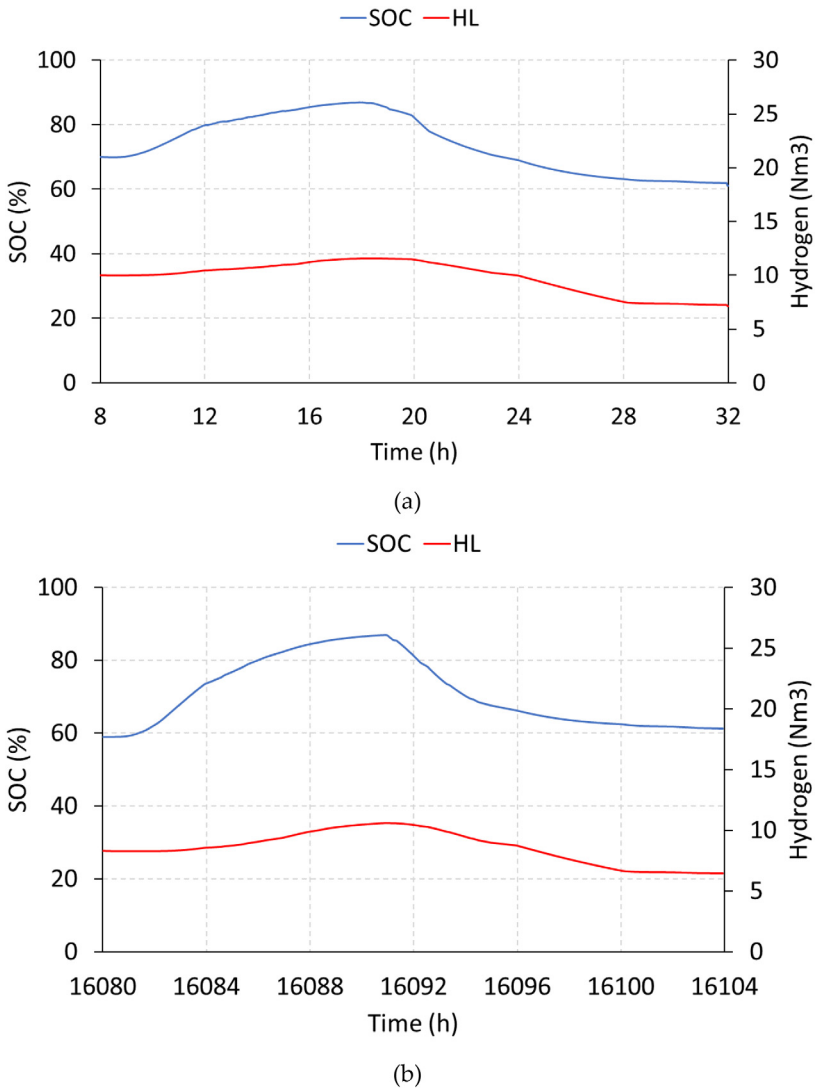

Fig. 11. Dynamics of the Battery SOC and HL managed by the developed EMS for (a) 8 h $\leq t \leq$ 32 h; and (b) 16080 h $\leq t \leq$ 16104 h.

Table 9
Degradation, losses and costs of the microgrid after full simulation.

EMS	HESS					MEG		
	Battery	Electrolyser	MSFC					
	Deg. (Ah)	Deg. (h)	Deg (V)		δDeg (V)	Losses (MWh)	Energy (kWh)	Cost (€)
			FC1	FC2				
Hyst-based EMS	2.514	1536.80	6.412	7.997	1.585	21.61	429.95	301.56
MPC-based EMS1	3.729	1687.70	3.741	4.506	0.765	29.95	159.35	−270.41
MPC-based EMS2	1.835	951.75	2.451	2.937	0.486	17.59	484.43	425.79
Developed EMS	1.125	1131.31	2.876	2.696	0.180	15.89	82.91	−28.56
Microgrid direct-connected to the MEG							2219.7	2259.86

between the electrolyser and the MEG. On the other hand, if the hydrogen level is low (HL (k) $\leq$ 10 N m^3), a greater use of the electrolyser is made to guarantee sufficient hydrogen for an energy deficit situation, see Fig. 10(a) for 9 h $\leq t \leq$ 17 h and (b) for 16081 h $\leq t \leq$ 16090 h.

In contrast, during the rest of the day, the microgrid is in an energy deficit situation: 17 h $\leq t \leq$ 32 h in Fig. 10(a), and 16090 h $\leq t \leq$ 16104 h in Fig. 10(b). As previously, it is the battery which firstly ensures the power balance, to reduce the degradation of the hydrogen system, and the MEG costs, see Fig. 10(a) (17 h $\leq t \leq$ 32 h). To keep the SOC within the required range, the EMS calculates the energy sharing between the MSFC system and the MEG according to the available HL, the accumulated degradation, the cost of purchasing energy, the power balance and its forecast. Then, assuming low degradation and medium value of HL, the developed EMS prioritizes the use of the MSFC system to reduce the MEG cost, see Fig. 10(a): 17 h $\leq t \leq$ 24 h. Conversely, if the HL is low, a greater use of the MEG is made, taking advantage of the low cost of purchasing energy during night-time hours, see Fig. 10(a): 24 h $\leq t \leq$ 32 h.

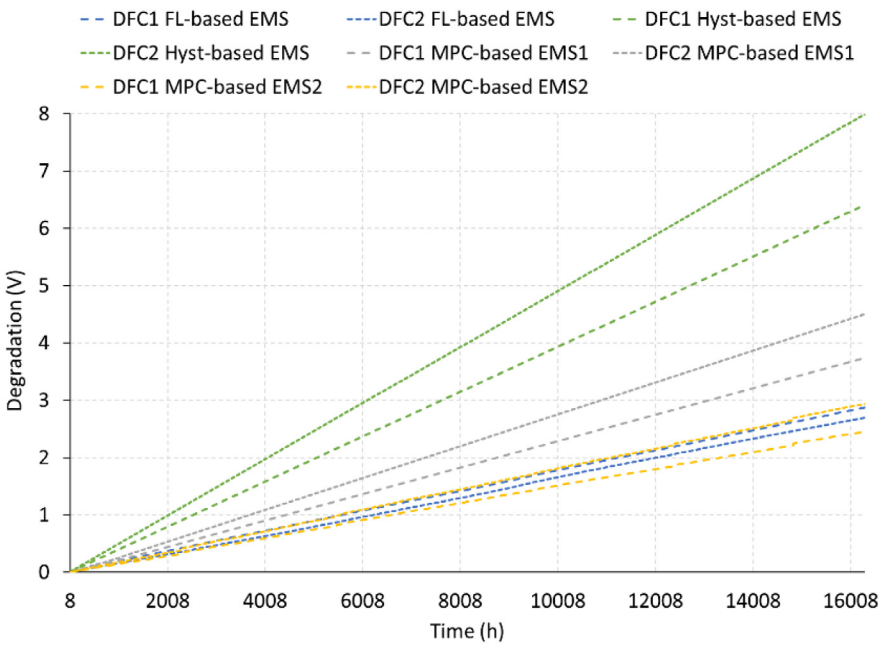

Fig. 12. Stacks 1 and 2 cumulative degradations for developed EMS versus reference EMSs.

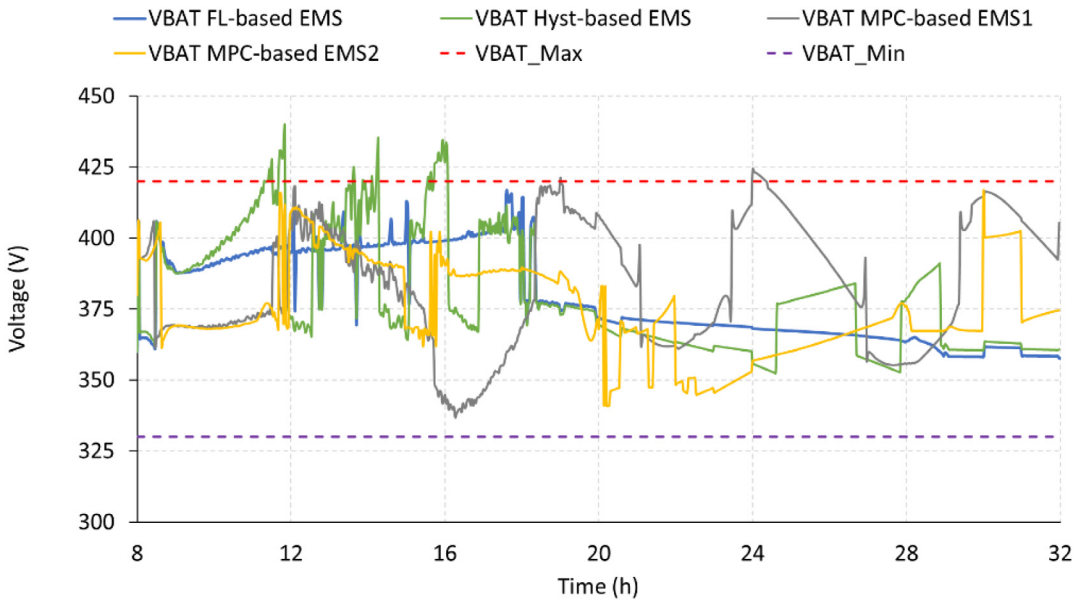

Fig. 13. Battery bank voltage profile for the developed EMS versus reference EMSs, as well as safety limits.

As discussed above, the energy exchange in the microgrid is strongly influenced by the degradation in the hydrogen system, therefore, increasing cumulative degradation of the stacks requires a more conservative use of the MSFC system, at the expense of a higher MEG usage and cost, see Fig. 10(b): 16090 h $\leq t \leq$ 16100 h.

For its part, the MSFC FLC (Figs. 2 and 3) calculates the energy distribution between the stacks based to their accumulated degradation, achieving a uniform degradation, regardless of the degradation ratios of the stacks, usually unknown in real cases, see Fig. 12.

Now, considering the degradation of the HESS (Table 9), the Hyst-based EMS and MPC-based EMS1 prioritizes the use of the microgrid's own resources to reduce the dependence on the MEG, which explains a considerably greater degradation of the microgrid equipment. Thus, respectively for these EMS, there are degradations of 2.51 Ah and 3,73 Ah for the battery bank, 1536,8 h and 1687.70 h of electrolyser operation, and 8 V (end of lifespan) and 4.50 V for the FC2 stack. In addition to the higher degradation of the stacks, it is not balanced, with degradation differences of 1.585 V and 0.765 V between stacks, equivalent to a difference of about 20%.

In contrast, the MPC-based EMS2 implements a more conservative approach to HESS utilization. In this case, the degradation of the battery bank reaches 1,83 Ah, while the electrolyser usage time is 951,75 h and a maximum degradation of the stacks (FC2) of approximately 2,93 V. Despite the benefits of conservative use of HESS, the degradation between stacks is again not homogeneous, a gap of 0.48 V is reached, equivalent to a difference of 15%. Finally, regarding the developed EMS, it reduces the degradation of the HESS and, in addition, in a balanced manner. Moreover, compared to the first two EMSs, the improvement in

the degradation of the battery bank is close to 225% and 330% for the Hyst-based EMS and the MPC-based EMS1 respectively. Moreover, the usage time of the electrolyser is reduced closely to 30%, and, regarding the MSFC system, its lifespan is almost doubled. Considering now the MPC-based EMS2, the developed EMS allows to achieve a more uniform response in terms of HESS lifespan. Thus, it allows a more conservative use of the battery bank (reduction of about 40%), with an increase in electrolyser usage time of only 15%. Finally, regarding the MSFC, the degradation ratios achieved are very similar (only 2% higher), however, in practice, both stacks are equally degraded, with a minimum degradation difference of only 0,18 V, equivalent to a difference of less than 7%.

Analysing the efficiency, the Hyst-based EMS calculates the operating power of the HESS based only on the level of stored energy. The MPC-based EMS1 prioritizes the use of microgrid resources with the objective of reducing dependence on MEG. In both cases, this leads to increased use of the hydrogen and battery ESSs; which are characterized by low and medium efficiency respectively. This causes, see Table 9, high losses with respect to the EMS developed, almost 40% for the EMS based on Hyst and almost 90% for the EMS1 based on MPC. Finally, the MPC-based EMS2 proposes a more restrictive use of the hydrogen system, to the detriment of greater use of the battery bank and the MEG, which allows an overall increase in the microgrid performance, but also a 10% increase in losses compared to the developed EMS.

On the other hand, as Table 9 shows, considering the usage and cost of the MEG at the end of the simulation, the use of the proposed microgrid architecture (Fig. 1) together with any of the compared EMSs, can greatly reduce the MEG dependence and costs compared to the exclusive use of the MEG (2219,67 kWh of energy expenditure and associated cost of 2259,86 €). The differences of the different EMS in terms of MEG costs are based on the following. The Hyst-based EMS limits the use of the MEG to situations of high deficit/excess of energy, without considering the electricity price. This often leads to buying/selling energy in economically unfavourable situations, which translates into MEG usage of 429,95 kWh, and cost of 301,56 €. Although the MPC-based EMS2 considers the MEG and the energy balance forecast, it establishes a more extensive use of the MEG with the objective of reducing the cumulative degradation of the hydrogen system. This translates into an increase in the energy flow between the microgrid and the MEG, up to a value of 484,43 kWh at a cost of 425,79 €. In the opposite direction, the MPC-based EMS1 establishes a control law that minimizes the cost of the connection to the MEG, consequently reaching a profit of approximately 270 €. However, the energy balance with the MEG is positive, with a value of 159,35 kWh, which entails a greater dependence on the MEG, and less use of the flexibility and degrees of freedom offered by the microgrid architecture. This is because the control law only minimizes the cost parameter, not the microgrid dependence of the MEG. On the opposite side, the developed EMS greatly reduce the use of the MEG (see Table 9), to the point of practically achieving energy independence from the MEG (only 3,7% of the energy required by the microgrid is imported), with a practically balanced cost/benefit.

Finally, although Table 9 shows the final degradation of each MSFC system stack for each compared EMS, something that has already been discussed, Fig. 13 shows the deterioration evaluation throughout the simulation. Note, on the one hand, the fast and unequal deterioration of the two stacks with the hyst-based EMS, and on the opposite side, the slow and equal deterioration of both stacks with the developed EMS (FL-based EMS). In the middle of the two commented EMS, less deterioration is observed in the MPC-based EMS1, and even less in the MPC-based EMS2, although in both cases it is unequal for the two stacks. With respect to Fig. 13, only the developed EMS (FL-based EMS) and MPC-based EMS2 are able to maintain the battery bank voltage, and thus the microgrid DC bus voltage, within the established safety range. However, the behaviour of the developed EMS is excellent with the lowest level of fluctuations.

6. Conclusions

This article presents a FL-based EMS for the energy management of residential-type DC microgrids with renewable generation, and which integrates the use of battery- and hydrogen-based HESS, as well as an MSFC system. The developed EMS has been designed to solve a multi-objective problem whose solution allows to increase the performance of the microgrid from a technical and economic point of view. Specifically, the EMS guarantees power balance in the microgrid while increasing the lifespan of its elements and the overall performance. For this, the developed EMS makes a conservative use of the hydrogen system, but, at the same time, regulates the exchange with the MEG to obtain the greatest economic profit. To this end, the developed EMS makes use of a hybrid control structure, consisting of a multivariable controller and event logic, as well as a local controller for the management of the MSFC system.

The developed EMS, at its different levels, incorporates expert knowledge for the definition of their fuzzy rule bases. The results obtained show that the developed EMS allows performance to be increased compared to the usual control solutions (reference in the bibliography) based on heuristic and model-based techniques. These results can be summarized as:

– An improvement in the response of the microgrid in global terms regarding the degradation, performance and connection costs to the MEG.

– A more conservative use of the HESS (to increase its lifespan), as well as of the MEG, which leads to a higher performance of the microgrid and a practically null annual average dependence on the MEG, without foregoing the economic benefit.

– Smooth and effective microgrid DC bus voltage control.

– A reduction and homogenization of the degradation of the stacks of the MSFC system.

From a quantitative point of view, compared to the reference techniques in the literature, the EMS developed based on FL allows to reduce the degradation of the battery bank and the MSFC system by up to 120% and 180%, respectively, compared to the double band hysteresis EMS, and up to 60% compared to strategies based on MPC. Considering the local controller based on FL, also developed in this work as part of the EMS, its use allows an excellent distribution of the degradation among the stacks, with practically the same level of degradation in all of them.

Considering the cost and use of the MEG, the developed EMS allows to decisively reduce the dependency and cost of the MEG, achieving a decrease of up to 90% in the use of the MEG with, in addition, a favourable economic balance. Finally, in terms of performance, the result obtained using the developed EMS allows to reduce up to 10% the losses in the operation of the microgrid with respect to the most favourable case of the EMS compared.

In summary, the developed EMS demonstrates that it is possible to solve a complex multi-objective problem efficiently and intuitively, without the need for complex models and, furthermore, with low computational cost, incorporating expert knowledge into a fuzzy controller. Future work will be aimed at improving the proposed solution, applying optimization techniques to the design of the membership functions of the fuzzy variables, as well as to the fuzzy rule bases of the controller. Also, to the application of techniques for the prediction of power and cost variables and their uncertainty.

List of Acronyms

DHW	Domestic how water.
DOD	Depth of discharge.
EMS	Energy management system.
ESS	Energy storage system.
EV	Electric vehicle.
FL, FLC	Fuzzy logic, fuzzy logic controller.
HESS	Hybrid energy storage system.
HA	House appliance.
HVAC	Heating, ventilating and air conditioning.
HL:	Hydrogen level.
MEG	Main electricity grid.
MPC	Model Predictive controller.
MSFC:	Multi-stack fuel cell.
PEM	Proton-exchange membrane.
PV	Photovoltaic.

Notation and Symbols

$C_{EP}(k)$	Cost of purchasing energy from the main electricity grid at sampling (€/Wh).
$C_{ES}(k)$	Cost of selling energy to the main electricity grid at sampling k (€/Wh).
$C_N\ (k)$	Rated battery capacity at sampling k (Ah).
$C_{MICRO}\ (k)$	Microgrid operating cost at sampling k (€).
$CYC_{FC}(k)$	Number of fuel cell operating cycles at sampling time k.
$D_{BAT}(k)$	Battery degradation at sampling k (Ah).
$D_{BAT_{Max}}$	Maximum battery degradation (Ah).
$D_{ELS}(k)$	Electrolyser degradation at sampling k (h).
$D_{ELS_{Max}}$	Maximum electrolyser degradation (h).
$D_{FCx}(k)$	Fuel cell stack x ($x = 1{,}2$) degradation (V).
$D_{FC_{Max}}$	Maximum fuel cell degradation (V/cell).
F	Faraday constant (96485 C/mol).
$HL\ (k)$	Hydrogen level (N m^3).
$H2_{ELS}\ (k)$	Electrolyser's hydrogen generation at sampling k (N m^3).
$H2_{FC}\ (k)$	MSFC's hydrogen consumption at sampling k (N m^3).
$I_{bat}\ (k)$	Battery current at sampling k (A).
ΔV_{CYC}	Fuel cell voltage drop considering the operating cycles (V/cycle/cell).
ΔV_{TIME}	Fuel cell voltage drop considering the operating hours (V/h/cell).
LHV	Hydrogen lower heating value (2993 Wh/N m^3).
$P_{BAT}\ (k)$	Battery bank power (W).
$P_{ELS}\ (k)$	Electrolyser power (W).
$P_{EV}\ (k)$	Electric vehicle demand (W).
$P_{FCx}(k)$	Fuel cell stack x ($x = 1, 2$) power (W).
P_{FC_N}	Nominal fuel cell power (W).
$P_{GRID_{IN}}\ (k)$	Power supplied from the MEG (W).
$P_{GRID_{OUT}}\ (k)$	Power supplied to the MEG (W).
$P_{GRID}\ (k)$	MEG power (W).
$P_{HVAC}\ (k)$	HVAC demand (W).
$P_{HESS}\ (k)$	HESS power (W).
$P_{H2}\ (k)$	Hydrogen system power (W).
$P_{H_{2ELS}}\ (k)$	Chemical power associated with the generated H_2 (W).
$P_{H_{2FC}}\ (k)$	Chemical power associated with the H_2 consumed (W).
$P_{LOAD}\ (k)$	Household appliance demand (W).
$P_{PV}\ (k)$	Renewable generation (PV panels) (W).
$P_{MSFC}(k)$	MSFC power (W).
$\eta_{BAT}\ (k)$	Overall battery efficiency at sampling k (%).
$\eta_{ELS}\ (k)$	Overall electrolyser efficiency at sampling k (%).
$\eta_{FC}\ (k)$	Overall fuel cell efficiency at sampling k (%).
$\eta_{GRID}\ (k)$	Overall grid efficiency at sampling k (95%).
$N_{cell_{ELS}}$	Number of cells of the electrolyser.
$N_{cell_{FC}}$	Number of cells fuel cell stack.
N_P	Prediction horizon.
N_U	Control horizon.
$S_{FCx}(k)$	Fuel cell stack x ($x = 1, 2$) state (ON/OFF).
$SOC\ (k)$	Battery state of charge.
T_s	Sampling period (h).
$V_{BAT}\ (k)$	Battery voltage at sampling k (V).
$V_{ELS}\ (k)$	Operating voltage of the electrolyser at sampling k (V).
$V_{FC}(k)$	Operating voltage of fuel cell (FC) at sampling k (V).
z	Number of electrons involved in the redox reaction ($z = 2$).

CRediT authorship contribution statement

F.J. Vivas: Conceptualization, Methodology, Formal analysis, Writing – original draft. **F. Segura:** Investigation, Conceptualization, Methodology, Writing – original draft. **J.M. Andújar:** Conceptualization, Writing – review & editing, Project administration, Supervision.

Declaration of competing interest

The authors declare that they have no known competing financial interests or personal relationships that could have appeared to influence the work reported in this paper.

Acknowledgements

This research was funded by "H2Integration&Control. Integration and Control of a hydrogen-based pilot plant in residential applications for energy supply" Spanish Government, grant Ref: PID2020-116616RB-C31", "SALTES: Smartgrid with reconfigurable Architecture for testing controL Techniques and Energy Storage priority" by Andalusian Regional Program of R+D+i, grant Ref: P20-00730, and by the project "The green hydrogen vector. Residential and mobility application", approved in the call for research projects of the Cepsa Foundation Chair of the University of Huelva. Funding for open access charge: Universidad de Huelva / CBUA.

References

[1] F.J. Vivas, A. De Las Heras, F. Segura, J.M. Andújar, A review of energy management strategies for renewable hybrid energy systems with hydrogen backup, Renew. Sustain. Energy Rev. 82 (2018) 126–155, http://dx.doi.org/10.1016/j.rser.2017.09.014.

[2] M. Jafari, Z. Malekjamshidi, D.D.C. Lu, J. Zhu, Development of a fuzzy-logic-based energy management system for a multiport multioperation mode residential smart microgrid, IEEE Trans. Power Electron. 34 (2019) 3283–3301, http://dx.doi.org/10.1109/TPEL.2018.2850852.

[3] F.K. Abo-Elyousr, J.M. Guerrero, H.S. Ramadan, Prospective hydrogen-based microgrid systems for optimal leverage via metaheuristic approaches, Appl. Energy 300 (2021) 117384, http://dx.doi.org/10.1016/j.apenergy.2021.117384.

[4] N. Herr, J.M. Nicod, C. Varnier, L. Jardin, A. Sorrentino, D. Hissel, et al., Decision Process to Manage Useful Life of Multi-Stacks Fuel Cell Systems Under Service Constraint, Vol. 105, Elsevier Ltd, 2017, http://dx.doi.org/10.1016/j.renene.2017.01.001.

[5] N. Marx, L. Boulon, F. Gustin, D. Hissel, K. Agbossou, A review of multi-stack and modular fuel cell systems: Interests, application areas and on-going research activities, Int. J. Hydrogen Energy 39 (2014) 12101–12111, http://dx.doi.org/10.1016/j.ijhydene.2014.05.187.

[6] A.J. Calderón, F.J. Vivas, F. Segura, J.M. Andújar, Integration of a multi-stack fuel cell system in microgrids: A solution based on model predictive control, Energies 13 (2020) http://dx.doi.org/10.3390/en13184924.

[7] K. Ullah, G. Hafeez, I. Khan, S. Jan, N. Javaid, A multi-objective energy optimization in smart grid with high penetration of renewable energy sources, Appl. Energy 299 (2021) 117104, http://dx.doi.org/10.1016/j.apenergy.2021.117104.

[8] F.J. Vivas, F. Segura, J.M. Andújar, J.J. Caparrós, A suitable state-space model for renewable source-based microgrids with hydrogen as backup for the design of energy management systems, Energy Convers. Manage. 219 (2020) 113053, http://dx.doi.org/10.1016/j.enconman.2020.113053.

[9] M.F. Zia, E. Elbouchikhi, M. Benbouzid, Microgrids energy management systems: A critical review on methods, solutions, and prospects, Appl. Energy 222 (2018) 1033–1055, http://dx.doi.org/10.1016/j.apenergy.2018.04.103.

[10] N. Bizon, M. Oproescu, M. Raceanu, Efficient energy control strategies for a standalone renewable/fuel cell hybrid power source, Energy Convers. Manage. 90 (2015) 93–110, http://dx.doi.org/10.1016/j.enconman.2014.11.002.

[11] M. Calderón, A.J. Calderón, A. Ramiro, J.F. González, Automatic management of energy flows of a stand-alone renewable energy supply with hydrogen support, Int. J. Hydrogen Energy 35 (2010) 2226–2235, http://dx.doi.org/10.1016/j.ijhydene.2009.12.028.

[12] T. Kamal, S.Z. Hassan, Hui Li, S.KL. Mumtaz, Energy management and control of grid-connected wind/ fuel cell/ battery hybrid renewable energy system, ICISE, Islamabad, 2016, pp. 1–6.

[13] C. Ziogou, D. Ipsakis, C. Elmasides, F. Stergiopoulos, S. Papadopoulou, P. Seferlis, et al., Automation infrastructure and operation control strategy in a stand-alone power system based on renewable energy sources, J. Power Sources 196 (2011) 9488–9499, http://dx.doi.org/10.1016/j.jpowsour.2011.07.029.

[14] D. Ipsakis, S. Voutetakis, P. Seferlis, F. Stergiopoulos, S. Papadopoulou, C. Elmasides, The effect of the hysteresis band on power management strategies in a stand-alone power system, Energy 33 (2008) 1537–1550, http://dx.doi.org/10.1016/j.energy.2008.07.012.

[15] J. Hu, Y. Shan, J.M. Guerrero, A. Ioinovici, K.W. Chan, J. Rodriguez, Model predictive control of microgrids – An overview, Renew. Sustain. Energy Rev. 136 (2021) 110422, http://dx.doi.org/10.1016/j.rser.2020.110422.

[16] A. Villalón, M. Rivera, Y. Salgueiro, J. Muñoz, T. Dragičević, F. Blaabjerg, Predictive control for microgrid applications: A review study, Energies 13 (2020) http://dx.doi.org/10.3390/en13102454.

[17] F. Garcia-Torres, A. Zafra-Cabeza, C. Silva, S. Grieu, T. Darure, A. Estanqueiro, Model predictive control for microgrid functionalities: Review and future challenges, Energies 14 (2021) 1–26, http://dx.doi.org/10.3390/en14051296.

[18] V.A. Freire, L.V.R. de Arruda, C. Bordons, J.J. Marquez, Optimal demand response management of a residential microgrid using model predictive control, IEEE Access 8 (2020) http://dx.doi.org/10.1109/ACCESS.2020.3045459.

[19] F.J. Vivas Fernández, F.S. Manzano, J.M.A. Márquez, A.J. Calderón Godoy, Extended model predictive controller to develop energy management systems in renewable source-based smart microgrids with hydrogen as backup. Theoretical foundation and case study, Sustainability 12 (2020) 1–28, http://dx.doi.org/10.3390/su12218969.

[20] M. Petrollese, L. Valverde, D. Cocco, G. Cau, J. Guerra, Real-time integration of optimal generation scheduling with MPC for the energy management of a renewable hydrogen-based microgrid, Appl. Energy 166 (2016) 96–106, http://dx.doi.org/10.1016/j.apenergy.2016.01.014.

[21] F. Garcia-torres, C. Bordons, Optimal economical schedule of hydrogen-based microgrids with hybrid storage using model predictive control, IEEE Trans. Ind. Electron. 62 (2015) 5195–5207, http://dx.doi.org/10.1109/TIE.2015.2412524.

[22] D. Yassuda Yamashita, I. Vechiu, J.P. Gaubert, Two-level hierarchical model predictive control with an optimised cost function for energy management in building microgrids, Appl. Energy 285 (2021) 116420, http://dx.doi.org/10.1016/j.apenergy.2020.116420.

[23] M. Castilla, C. Bordons, A. Visioli, Event-based state-space model predictive control of a renewable hydrogen-based microgrid for office power demand profiles, J. Power Sources 450 (2020) 227670, http://dx.doi.org/10.1016/j.jpowsour.2019.227670.

[24] L. Valverde, F. Rosa, C. Bordons, J. Guerra, Energy management strategies in hydrogen smart-grids: A laboratory experience, Int. J. Hydrogen Energy 41 (2016) 13715–13725, http://dx.doi.org/10.1016/j.ijhydene.2016.05.279.

[25] A.J. Barragan, J.M. Enrique, F. Segura, J.M. Andujar, Iterative fuzzy modeling of hydrogen fuel cells by the extended Kalman filter, IEEE Access 8 (2020) 180280–180294, http://dx.doi.org/10.1109/ACCESS.2020.3013690.

[26] J.M. Andújar, A.J. Barragán, M.E. Gegúndez, M. Maestre, Multivariable fuzzy control system based on heuristic. A practical subject: Container crane control, RIAI - Rev. Iberoamericana de Autom. E Inform. Ind. 4 (2007) http://dx.doi.org/10.1016/s1697-7912(07)70212-1.

[27] P. Garcia-Trivino, J.P. Torreglosa, L.M. Fernandez-Ramirez, F. Jurado, Decentralized fuzzy logic control of microgrid for electric vehicle charging station, IEEE J. Emerg. Sel. Top. Power Electron. 6 (2018) 726–737, http://dx.doi.org/10.1109/JESTPE.2018.2796029.

[28] D. Arcos-Aviles, J. Pascual, L. Marroyo, P. Sanchis, F. Guinjoan, Fuzzy logic-based energy management system design for residential grid-connected microgrids, IEEE Trans. Smart Grid 9 (2018) 530–543, http://dx.doi.org/10.1109/TSG.2016.2555245.

[29] D. Arcos-Aviles, J. Pascual, F. Guinjoan, L. Marroyo, G. Garcia-Gutierrez, R. Gordillo-Orquera, et al., An energy management system design using fuzzy logic control: Smoothing the grid power profile of a residential electro-thermal microgrid, IEEE Access 9 (2021) 25172–25188, http://dx.doi.org/10.1109/ACCESS.2021.3056454.

[30] M.H. Athari, M.M. Ardehali, Operational performance of energy storage as function of electricity prices for on-grid hybrid renewable energy system by optimized fuzzy logic controller, Renew. Energy 85 (2016) 890–902, http://dx.doi.org/10.1016/j.renene.2015.07.055.

[31] P. García, J.P. Torreglosa, L.M. Fernández, F. Jurado, Optimal energy management system for stand-alone wind turbine/photovoltaic/ hydrogen/battery hybrid system with supervisory control based on fuzzy logic, Int. J. Hydrogen Energy 38 (2013) 14146–14158, http://dx.doi.org/10.1016/j.ijhydene.2013.08.106.

[32] N. Nabipour, S.N. Qasem, K. Jermsittiparsert, Type-3 fuzzy voltage management in PV/Hydrogen fuel cell/battery hybrid systems, Int. J. Hydrogen Energy 45 (2020) 32478–32492, http://dx.doi.org/10.1016/j.ijhydene.2020.08.261.

[33] P.B. Nempu, N. Sabhahit Jayalakshmi, A new power management strategy for PV-FC-based autonomous DC microgrid, Arch. Electr. Eng. 67 (2018) 815–828, http://dx.doi.org/10.24425/aee.2018.124742.

[34] T. Vigneysh, N. Kumarappan, Autonomous operation and control of photovoltaic/ solid oxide fuel cell/ battery energy storage based microgrid using fuzzy logic controller, Int. J. Hydrogen Energy 41 (2016) 1877–1891.

[35] M.H. Cano, S. Kelouwani, K. Agbossou, Y. Dubé, Power management system for off-grid hydrogen production based on uncertainty, Int. J. Hydrogen Energy 40 (2015) 7260–7272, http://dx.doi.org/10.1016/j.ijhydene.2015.03.157.

[36] M. Jafari, Z. Malekjamshidi, J. Zhu, M.H. Khooban, A novel predictive fuzzy logic-based energy management system for grid-connected and off-grid operation of residential smart microgrids, IEEE J. Emerg. Sel. Top. Power Electron. 8 (2020) 1391–1404, http://dx.doi.org/10.1109/JESTPE.2018.2882509.

[37] S.S. Zehra, A. Ur Rahman, I. Ahmad, Fuzzy-barrier sliding mode control of electric-hydrogen hybrid energy storage system in DC microgrid: Modelling, management and experimental investigation, Energy 239 (2022) http://dx.doi.org/10.1016/j.energy.2021.122260.

[38] I. Abadlia, T. Bahi, H. Bouzeria, Energy management strategy based on fuzzy logic for compound RES/ESS used in stand-alone application, Int. J. Hydrogen Energy 41 (2016) 16705–16717, http://dx.doi.org/10.1016/j.ijhydene.2016.07.120.

[39] F. Keskin Arabul, A.Y. Arabul, C.F. Kumru, A.R. Boynuegri, Providing energy management of a fuel cell–battery–wind turbine–solar panel hybrid off grid smart home system, Int. J. Hydrogen Energy 42 (2017) 26906–26913, http://dx.doi.org/10.1016/j.ijhydene.2017.02.204.

[40] G. Kyriakarakos, A.I. Dounis, K.G. Arvanitis, G. Papadakis, A fuzzy logic energy management system for polygeneration microgrids, Renew. Energy 41 (2012) 315–327, http://dx.doi.org/10.1016/j.renene.2011.11.019.

[41] S. Al-Sakkaf, M. Kassas, M. Khalid, M.A. Abido, An energy management system for residential autonomous DC microgrid using optimized fuzzy logic controller considering economic dispatch, Energies 12 (2019) http://dx.doi.org/10.3390/en12081457.

[42] F.J. Vivas, F. Segura, J.M. Andújar, A. Palacio, J.L. Saenz, F. Isorna, et al., Multi-objective fuzzy logic-based energy management system for microgrids with battery and hydrogen energy storage system, Electronics (Switzerland) 9 (2020) 1–25, http://dx.doi.org/10.3390/electronics9071074.

[43] J.M. Enrique, E. Dura, Theoretical assessment of the maximum power point tracking efficiency of photovoltaic facilities with different converter topologies, Sol. Energy 81 (2007) 31–38, http://dx.doi.org/10.1016/j.solener.2006.06.006.

[44] J.M. Enrique, J.M. Andújar, M.A. Bohórquez, A reliable, fast and low cost maximum power point tracker for photovoltaic applications, Sol. Energy 84 (2010) 79–89, http://dx.doi.org/10.1016/j.solener.2009.10.011.

[45] J.M. Andújar, F.J. Vivas, F. Segura, A.J. Calderón, Integration of air-cooled multi-stack polymer electrolyte fuel cell systems into renewable microgrids, Int. J. Electr. Power Energy Syst. 142 (2022) http://dx.doi.org/10.1016/j.ijepes.2022.108305.

[46] J.B. Copetti, E. Lorenzo, F. Chenlo, A general battery model for PV system simulation, Prog. Photovolt., Res. Appl. 1 (1993) 283–292, http://dx.doi.org/10.1002/pip.4670010405.

[47] S. Dhundhara, Y.P. Verma, A. Williams, Techno-economic analysis of the lithium-ion and lead–acid battery in microgrid systems, Energy Convers. Manage. 177 (2018) 122–142, http://dx.doi.org/10.1016/j.enconman.2018.09.030.

[48] A. Kosonen, J. Ahola, M. Niemelä, J. Koponen, K. Huoman, V. Ruuskanen, Control and energy efficiency of PEM water electrolyzers in renewable energy systems, Int. J. Hydrogen Energy 42 (2017) 29648–29660, http://dx.doi.org/10.1016/j.ijhydene.2017.10.056.

[49] Y. Zhang, W. Wei, Decentralized coordination control of PV generators, storage battery, hydrogen production unit and fuel cell in islanded DC microgrid, Int. J. Hydrogen Energy 45 (2020) 8243–8256, http://dx.doi.org/10.1016/j.ijhydene.2020.01.058.

[50] Instituto para la Diversificación y Ahorro de la Energía (IDAE), Ministerio de industria energía y turismo. Consumo por usos del sector residencial, 2022, https://informesweb.idae.es/consumo-usos-residencial/informe.php.

[51] F.J. Vivas, A. De las Heras, F. Segura, J.M. Andújar, H2RES2 simulator. A new solution for hydrogen hybridization with renewable energy sources-based systems, Int. J. Hydrogen Energy 42 (2017) 13510–13531, http://dx.doi.org/10.1016/j.ijhydene.2017.02.139.

[52] F. Garcia-Torres, C. Bordons, Optimal economical schedule of hydrogen-based microgrids with hybrid storage using model predictive control, IEEE Trans. Ind. Electron. 62 (2015) 5195–5207, http://dx.doi.org/10.1109/TIE.2015.2412524.

[53] L. Valverde, C. Bordons, F. Rosa, Integration of fuel cell technologies in renewable-energy-based microgrids optimizing operational costs and durability, IEEE Trans. Ind. Electron. 63 (2016) 167–177, http://dx.doi.org/10.1109/TIE.2015.2465355.